European Commission
FP7, Grant Agreement 211743

Materials and components of possible interest for cryogenic operation of Einstein Telescope

ET-026-09

R. Poggiani

Issue: 1

Date: 29 October 2009

University of Pisa and INFN Pisa

ET – Einstein gravitational wave Telescope – Design Study * A joint European Project
Web: http://www.et-gw.eu Email: EuropeanProjectsService@ego-gw.it

Contents

1 Introduction

The aim of this report is to review some possible materials and components for cryogenic operation of Einstein Telescope, with a special focus on suspensions. The properties of materials at low temperature are summarized in the next section. The following sections deal with specific blocks of Einstein Telescope: actuators, cabling, adhesives and magnets. We will make no preliminary hypothesis about the operation temperature of each block, reporting the literature data over the widest possible range. As a general guideline, the recommended materials for use in cryogenic environments are: 300–series austenitic steels (in particular 304LN and 316LN); austenitic alloys (in particular Fe–Ni–Cr–N and Fe–Mn–Cr–N alloys and Inconel 908); OFHC copper and deoxidized copper; Al alloys (6061, 6063, 1100); titanium; niobium; Invar; Kapton; quartz. Materials not recommended for cryogenic use are: martensitic steels (undergo ductile to brittle transition); carbon steels; plastics. According to these prescriptions, some components of suspension system can work down to liquid helium temperature

without changes, such as filter and marionetta bodies. The thermal expansion coefficient of all parts working at cryogenic temperatures must be carefully tuned. The assembled components for which cryogenic operation is foreseen, should be tested firstly at 77 K, where most of thermal contraction occurs, and at 4.2 K if necessary. Other materials, such as the blade material should be separately studied in cas cryogenic operation is foreseen. Some maraging steels have been tested at cryogenic temperatures. The 18Ni 200 grade maraging steel was tested at room temperature and at -170^{0}C: the fracture was ductile at both temperatures, but the fatigue crack growth rate at -170^{0}C was half the value at room temperature.

The report is based on the Virgo notes VIR-NOT-PIS-1390-272, VIR-NOT-PIS-1390-299, VIR-NOT-PIS-1390-310, VIR-NOT-PIS-1390-340, VIR-060B-08, VIR-0563A-09.

2 Material properties at low temperatures

2.1 Heat transfer

Heat transfer at low temperatures [1], [2], [3] mainly occurs through conduction in the residual gas and the solids connecting the cold parts to exterior and through radiation. Since Einstein Telescope will operate in high vacuum, convection will be eliminated. The mean free path of molecules at low pressures is of the order of one meter at 10^{-4} mbar. In this case, the thermal conductivity is proportional to the number of molecules and to their mean velocity. In the special case of two parallel surfaces at temperatures T_1, T_2 the heat $\dot{Q}$ transferred by conduction in a gas at pressure p is:

$$\dot{Q} = \frac{a_0}{4}\frac{\gamma+1}{\gamma-1}\sqrt{\frac{2R}{\pi M}}p\frac{T_2-T_1}{\sqrt{T}} \tag{1}$$

where T is the temperature at the pressure gauge, M is the molecular weight and:

$$a_0 = \frac{a_1 a_2}{a_2 + \frac{A_1}{A_2}(1-a_2)a_1} \tag{2}$$

where a_i are the accomodation coefficients of molecules on the surfaces, A_i the areas; generally the accomodation coefficient for clean gas free surfaces increases with molecular weight.

For a material with section A under a temperature gradient $\frac{\partial T}{\partial x}$ the heat transfer by conduction is:

$$\dot{Q} = \lambda(T)A\frac{\partial T}{\partial x} \tag{3}$$

where $\lambda(T)$ is the thermal conductivity. Thermal conductivity is the key parameter when designing a thermal link or for heat sinking. Data for several materials with different levels of conductivity are shown in Fig. 1. The thermal conductivity at low temperatures behaves as bT^3 for insulators (phonon conductivity) and as k_0T for metals (electron conductivity).

In practical design it is common to use a mean thermal conductivity between temperature pairs:

$$\bar{\lambda} = \frac{1}{T_2-T_1}\int_{T_1}^{T_2}\lambda(T)dT \tag{4}$$

The conductivity depends on the chemical and physical state of material and on its history, thus using average values for materials is not recommended. For example, the thermal conductivity of metals can be enhanced by one order of magnitude by annealing in oxygen (10^{-2} mbar pressure) at 700^{0}C for 24 hours.

In the following, I will restrict the discussion to the materials mostly used for thermal links: copper and aluminum. The thermal conductivity of Oxigen–Free–High–Conductivity copper (OFHC) samples with residual resistivity ratios RRR (ratio of the resistivity at 300 K and at 4.2 K; it is also an indicator of material purity)

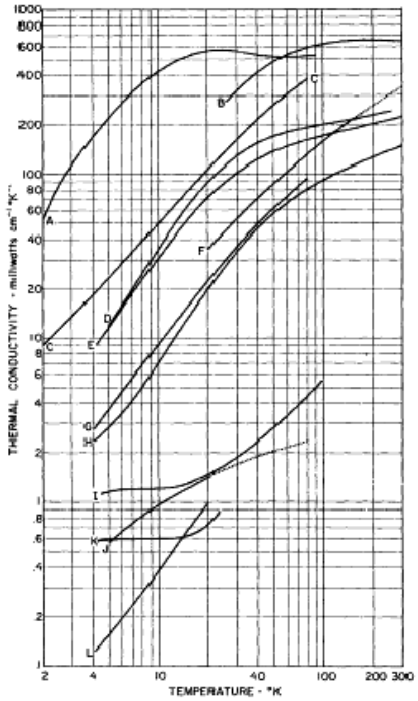

FIGURE 10.8. Low-temperature thermal conductivities of some solids with relatively low conductivities. A, 50-50 lead-tin solder [44]; B, steel, SAE 1020 [39]; C, beryllium copper [44]; D, constantan [39]; E, Monel® [39]; F, silicon bronze [42]; G, Inconel® [39]; H, type 347 stainless steel [39]; I, fused quartz [39]; J, polytetrafluoroethylene (Teflon®) [41]; K, polymethylmethacrylate (perspex) [39]; L, nylon [44].

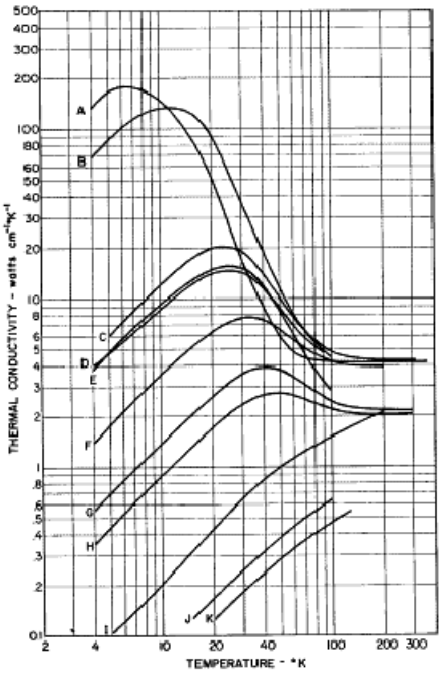

FIGURE 10.7. Low-temperature thermal conductivities of some metals having relatively high conductivities. A, silver 99.999% pure [39]; B, high purity copper [42]; C, coalesced copper [42]; D, copper, electrolytic tough pitch [42]; E, aluminum single crystal [43]; F, free-machining tellurium copper [42]; G, aluminum, 1100 F [43]; H, aluminum, 6063-T5 [43]; I, copper, phosphorus deoxidized [42]; J, aluminum, 2024-T4 [43]; K, free-machining leaded brass [42].

Figure 1: Thermal conductivity of materials with relatively low and relatively high conductivity [2]

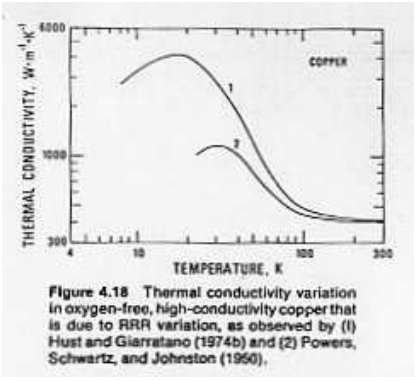

Figure 4.18 Thermal conductivity variation in oxygen-free, high-conductivity copper that is due to RRR variation, as observed by (1) Hust and Giarratano (1974b) and (2) Powers, Schwartz, and Johnston (1960).

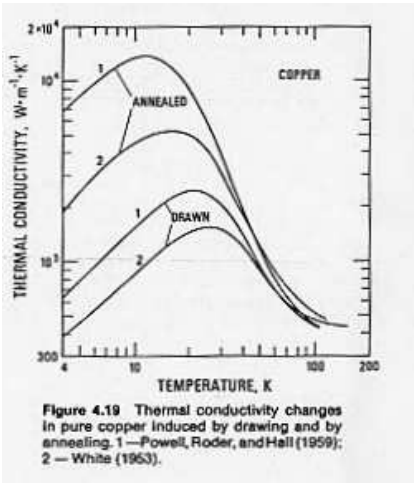

Figure 4.19 Thermal conductivity changes in pure copper induced by drawing and by annealing. 1—Powell, Roder, and Hall (1959); 2 — White (1953).

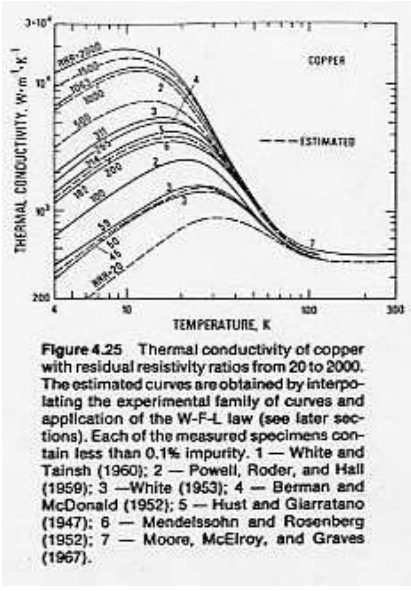

Figure 4.25 Thermal conductivity of copper with residual resistivity ratios from 20 to 2000. The estimated curves are obtained by interpolating the experimental family of curves and application of the W-F-L law (see later sections). Each of the measured specimens contain less than 0.1% impurity. 1 — White and Tainsh (1960); 2 — Powell, Roder, and Hall (1959); 3 —White (1953); 4 — Berman and McDonald (1952); 5 — Hust and Giarratano (1947); 6 — Mendelssohn and Rosenberg (1952); 7 — Moore, McElroy, and Graves (1967).

Figure 2: Left: thermal conductivity of OFHC copper with RRR values of 214 (top curve) and 35 (bottom curve) [3]; center: variation of thermal conductivity of copper under drawing and annealing [3]; right: thermal conductivity of copper with different purity [3]

of 35 and 214 is shown in Fig. 2, left. Drawing and annealing have an effect on thermal conductivity: the difference between a copper drawn wire and a drawn and annealed wire is shown in Fig. 2, center. The purity level determines a great spread in the thermal conductivity of copper, as shown in Fig. 2, right.

The thermal conductivity of aluminum alloys with different purities is shown in Fig. 3.

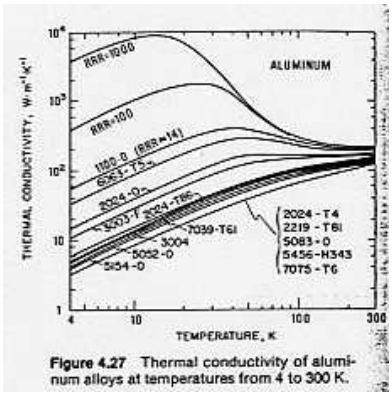

Figure 4.27 Thermal conductivity of aluminum alloys at temperatures from 4 to 300 K.

Figure 3: Thermal conductivity of aluminum alloys with different purity [3]

The LCGT collaboration has recently investigated [4] the effect of size on the thermal conductivity of pure Al and pure Cu, materials to be used in the wires for the heat links between an intermediate mass at 14 K and an heat shield at 8 K. No size effect was found for wire diameters above 0.2 mm. The observed thermal conductivity of aluminum with RRR of 5000 was 2×10^4 W/m/K. The quality factor of samples at 8 K (deduced from the pendulum quality factor) was 345.6 for Al and 1623 for copper.

While copper and aluminum are the appropriate choice for thermal links, thermal isolation is achieved using Al_2O_3 or Vespel SP–22 (loaded with graphite).

The thermal conductivity and the electrical resistivity ρ are related by the Wiedemann–Franz–Lorenz law:

$$\lambda\rho = LT \tag{5}$$

where L is the Lorenz number.

The heat transfer by radiation in cryogenics does not involve black bodies only, but generally surfaces with smaller emissivity. Metal emissivities are in the range 0.02–0.6 for copper, 0.02–0.3 for aluminum, 0.05–0.1 for stainless steel. For two plane parallel surfaces of area A at temperatures T_1, T_2, with emissivities ε_1, ε_2, the heat transfer by radiation is:

$$\dot{Q} = \sigma A(T_1^4 - T_2^4)\frac{\varepsilon_1\varepsilon_2}{\varepsilon_1 + \varepsilon_2 - \varepsilon_1\varepsilon_2} \tag{6}$$

At low temperatures, heat radiation is not an efficient mechanism for cooling. However, heat transfer by radiation from hot to cold surfaces demands radiation shields.

An additional source of heat transfer is the Joule heating $\dot{Q} = RI^2$ of electrical connections, in addition to heat transport through the cabling. Given the great number of control and sensing systems in Einstein Telescope, this aspect must be carefully engineered, considering also the constraint of low mechanical stiffness required to avoid noise injection. Optimization of the geometry, dissipation and thermal anchoring of cabling is needed. The electrical connections must fulfill the opposite requirements of low thermal conductivity and low electrical resistivity at the same time. The electrical resistivity of metals decreases by two orders of magnitude from 300 to 4.2 K, while the thermal conductivity has a maximum at one twentieth of the Debye temperature θ and a linear decrease below. On the other hand, the electrical resistivity of alloys is weakly decreasing from 300 to 4.2 K, while the thermal conductivity is decreasing by one or two orders of magnitude. The topic is addressed in detail in section 4.

Other quantities of interest for cryogenic work are specific heat, thermal expansion coefficient and Young modulus.

The specific heat at constant volume of most solids is described by the Debye function:

$$C_V = 9R\left(\frac{T}{\theta}\right)^3 \int_0^{\frac{\theta}{T}} \frac{x^4}{(e^x-1)(1-e^{-x})} dx \tag{7}$$

where $x = \frac{h\nu}{kT}$. The quantity is related to specific heat at constant pressure by the equation:

$$C_P - C_V = VT\frac{\beta^2}{\chi} \tag{8}$$

where β, χ are the volumic expansion coefficient and the compressibility. Specific heat is generally decreasing with decreasing temperature: the advantage is the increase of cooling speed with decreasing temperature, the disadvantage is that small heat leaks can produce large temperature increases. The specific heat of some materials is reported in Fig. 4.

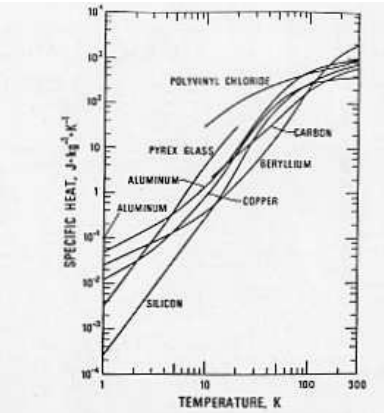

Figure 2.1 Specific heat as a function of temperature for several types of material. Typical behaviors are illustrated for metals (aluminum, beryllium, and copper), semiconductors (carbon and silicon), an amorphous inorganic (Pyrex glass) (Cerruccini and Gniewek, 1960), and for an organic polymer (polyvinyl chloride) (Chang, 1977). A single point is shown for aluminum in the superconducting state at 1 K.

Figure 4: Specific heat of some materials [3]

Thermal contraction is an important factor for cryogenic mechanical construction and reliability. The contraction at low temperatures can produce gaps or crossing of different parts and in general a strain increase. For metal rods the thumb rule is a contraction of a few mm/m between 300 and 4 K. The most part of contraction occurs between 300 and 77 K: a test with liquid nitrogen is useful as a preliminary validation of mechanical reliability. The relative linear thermal expansion coefficient of several materials when cooled from room temperature to lower temperatures is shown in Fig. 5.

The expansion coefficient α and the specific heat at constant volume are related by the Grüneisen equation:

$$3\alpha = \gamma\chi c_v \tag{9}$$

where c_v is the specific heat per unit volume, χ the compressibility, γ the Grüneisen constant.

The strength of several materials increases with decreasing temperature as long as ductile to brittle transition does not occur. The Young modulus of some metals is shown in Fig. 6.

For some materials, published data could be enough for design. The thermal conductivity and the thermal expansion coefficients of critical materials, such as the suspension fibers, heat links etc must be separately tested.

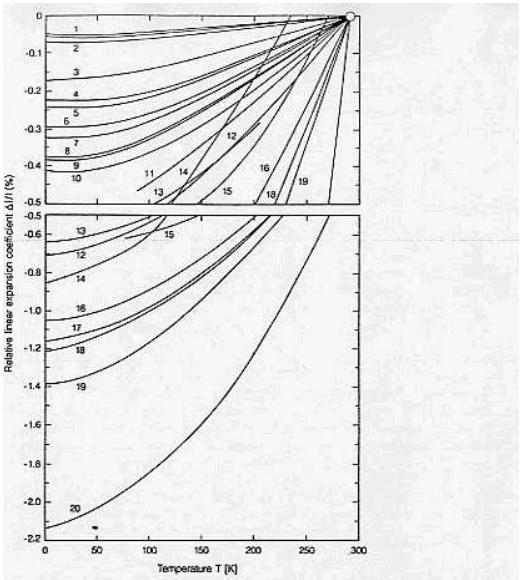

Fig.3.14. Relative linear thermal expansion coefficient of (1) Invar (upper), Pyrex (lower), (2) W, (3) non-alloyed steel, (4) Ni, (5) $Cu_{0.7}Ni_{0.3}$, (6) stainless steel, (7) Cu, (8) German silver, (9) brass, (10) Al, (11) soft solder, (12) In, (13) Vespel SP22, (14) Hg, (15) ice, (16) Araldite, (17) Stycast 1266, (18) PMMA, (19) Nylon, (20) Teflon [3.44]. Some further data are: Pt similar to (3); Ag between (9) and (10); Stycast 2850 GT slightly larger than (10). The relative change of length between 300 and 4 K is $10^3 \Delta\ell/\ell$ = 11.5, 4.2, 6.3 and 5.7 for Stycast 1266, Stycast 2850 GT, Vespel SP-22 and solders, respectively [3.43-45]

Figure 5: Relative linear thermal expansion coefficient of different materials [2]

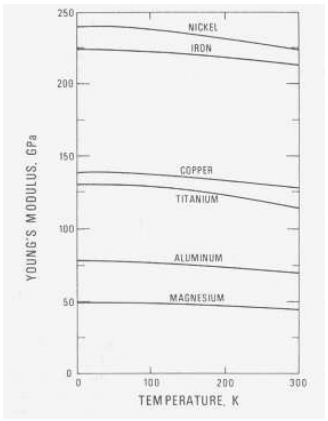

Figure 6: Young modulus of some metals [3]

2.2 Thermal conductivity

Thermal conductivity is usually measured using a simple geometry, that is rod shaped samples. The total heat conduction $\dot{Q}$ in a solid rod of cross section A and length L is defined as [1]:

$$\dot{Q} = \frac{A}{L} \int_{T_0}^{T_1} \lambda(T) dT \tag{10}$$

where λ is the thermal conductivity, generally with a complicate dependence on temperature: for this reason a differential measurement is needed. The standard method of longitudinal heat flow uses a thermal bath and a pair of thermometers. A simple solution to measure thermal conductivity at 77 K and 4.2 K is mounting the sample inside an evacuated chamber immersed in the cryogenic liquid (nitrogen or helium). Since both 77

and 4.2 K are fixed points of liquified gases and are typical points of operation of pulse tubes, achieving and maintaining the working temperature is not a big deal. The sample is fixed to the chamber wall on one end and has an heater attached to the other end. To achieve a good thermal contact and practical mounting, the sample is fitted with copper clamps at both ends. Two thermometers are used to probe temperature in two points: it is suggested to use calibrated thermometers. Semiconductor and carbon–glass thermometers are the standard choice for thermometry below some tens K. An improvement in precision can be achieved working with the method by National Bureau of Standards, where eight sensors along the rod sample are used to get the final value by the weighted average.

The longitudinal heat flow method has been used by [5] to measure the heat transfer along thin sapphire fibers and could be used for testing silicon fibers for cryogenic operation of Einstein Telescope. The apparatus is shown in Fig. 7: the bottom heater produced a temperature gradient in the fiber, measured by two carbon–glass resistors, while the top heater was used to vary the base temperature of sample. The components were inside an evacuated chamber immersed in a cryogenic liquid.

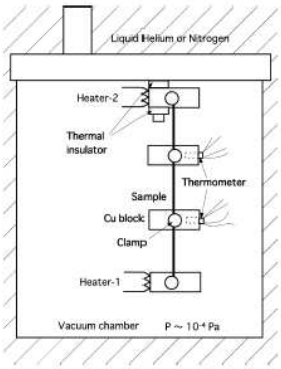

Figure 7: Apparatus used by [5] to measure the thermal conductivity of sapphire fibers

The thermal conductivity of material is described by $\lambda = c_V v_s l/3$, where c_V is the volumic specific heat, v_s the sound speed in the material, l the phonon mean free path. In thin fibers at cryogenic temperatures the mean free path can be limited by boundary scattering.

2.3 Thermal expansion

According to the type of material, different techniques are available [6] to measure thermal expansion coefficient. The most intuitive is the use of strain gauges, where the change of sample length is measured by the deformation of a membrane sensed by the strain gauge [7], see Fig. 8, top left. The signal is the variation of the gauge resistance. If the strain gauge is mounted on a sample not subject to stress, there is still a variation of the resistance due to the temperature dependence. The thermal output strain includes not only the contribution of sample expansion, but also the temperature dependence effect: thus the strain must be compensated. The technique has been used for copper and alloys down to a few Kelvin. The quoted minimum detectable change in sample thickness is some hundreds Å. Cryogenic strain gauges are commercially available.

The thermal expansion of metal samples can be tested from the capacitance variation due to change in sample dimension. The basic principle is having a capacitor whose capacity is determined by the distance between a sample and a reference copper element: one plate is fixed and the other is on the sample itself. The capacitor is used inside the tank circuit of a rf oscillator, thus the variation in length, transformed into a capacity variation, becomes a frequency variation. A refined and more precise version of the two terminal technique is the three terminal capacitor technique, especially suitable for the lowest temperatures. An absolute instrument based on this technique [8] is shown in Fig. 8, top right. This technique has been used for aluminium, copper and other metals. The minimum detectable change in the sample thickness is of the order of 0.1 Å.

The variable transformer technique [9] is absolute. The primary coil of transformer is in the low temperature part of the setup, while the secondary is fixed to the sample but it is isolated and inside a glass vacuum can; for details, see Fig. 8, bottom left. The only part whose properties are varying with temperature is the sample itself, causing the mutual inductance to vary, with a linear dependence on the position: the variation is measured with an inductance bridge. The minimum detectable thickness change is of the order of 0.1 Å. The application of this method has been restricted to high conductivity materials: copper, aluminium, sapphire etc.

The thermal expansion coefficient of silicon and CaF_2, materials under consideration for suspensions, have been measured down to a few Kelvin by [10] using the X–ray method. This techniques measures the absolute distance d between crystal planes. When the crystal is heated the distance between planes increases; it is measured applying the Bragg law: $n\lambda = 2d \sin\theta$, where λ is the incident radiation wavelength. The method has been used also with aluminium, copper, germanium etc, generally with a rotating X–camera, see Fig. 8, bottom right. The achievable relative precision on the lattice thermal expansion is of the order of 5×10^{-6}.

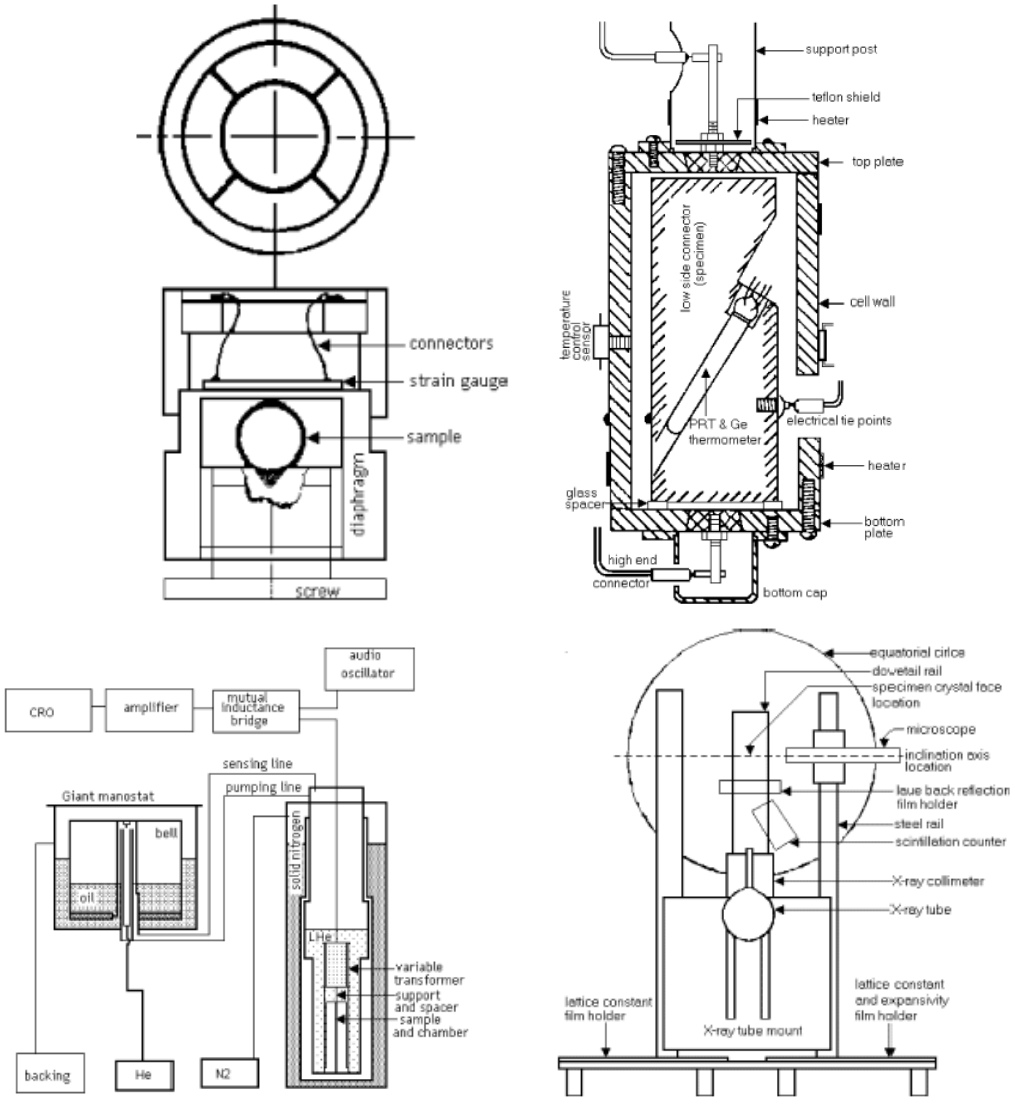

Figure 8: Measurement of thermal expansion coefficient: strain gauge method [7] (top left); capacitance method [8] (top right); variable transformer technique [9] (bottom left); X–ray technique [10] (bottom right)

The last technique is attractive since allows to get detailed information about the crystal characteristics, but at the cost of an increased complexity of the apparatus.

2.4 Cryogenic creep

Significant creep at cryogenic temperatures has been observed in several materials, including metals [11]. The total strain in the material is described by the superposition of the instantaneous tensile strength on loading and a time dependent creep strain, including the primary creep, the steady state creep and the tertiary creep, see Fig. 9.

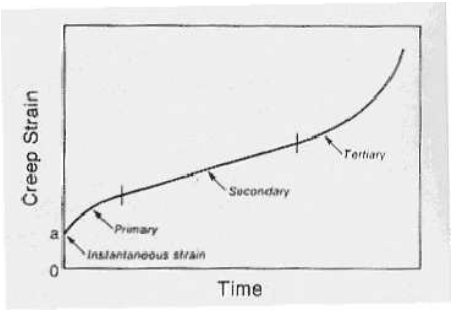

Figure 9: Creep curve versus time

The earlier studies of cryogenic creep were short term tests lasting a few hours at most and investigating transient creep:

$$\varepsilon = \alpha \ln(\gamma t + 1) \tag{11}$$

where ε is the creep strain, t the time and the α, γ parameters depend on the material and the test conditions. For some time it was assumed that cryogenic creep was exhaustive and the further steps of creep were not observable. The creep curve of OFHC at 77 K in Fig. 10, left, shows a very long (50 hours) transient and a steady state longer than 100 hours. The creep curves at liquid helium temperature in Fig. 10, center, exhibit transient creep only. Creep speed is governed by an Arrhenius equation with a characteristic activation energy. If this quantity is independent from temperature, the extrapolation of the equation should lead to negligible creep rates at liquid nitrogen or liquid helium temperatures. However, this is not the case as show in Fig. 10, right. The steady state creep observed at liquid nitrogen temperature is higher than the extrapolation by several orders of magnitude. The slope change at different temperatures is a consequence of a change in the creep mechanism, thus in the activation energy.

I will briefly recall cryogenic creep data for steels. The data refer to the transient stage of creep. For a value of the quantity r (ratio of the stress to the yield strength) above 1 the α coefficients is in the range $(0.9–16)\times10^{-4}$ at 20 K and in the range $(7.4–30)\times10^{-4}$ at 77 K; for a value below 1 it is in the range $(0.35–2.7)\times10^{-4}$ at 77 K [11]. Another material that has been considered for suspensions is niobium: the α coefficient is in the range $(43–300)\times10^{-4}$ for temperatures 84-300 K [11]. The behavior of activation energy of the creep process demands specific measurements at the required operation temperatures and for some hundreds hours. The creep test apparatus must provide load stability and temperature stability (from 4.2 K to room temperature) during the whole test. The vibration input must be minimized, due to the smallness of the effect under investigation. A pulse tube can be considered for this test. In these tests there is an additional requirement with respect to the other measurements: the necessity of transmitting stress to the sample. In the standard procedure, the cold chamber in the cryostat contains a tensile testing insert and is equipped with a constant load creep machine. Strain gauges have been used in the past to measure the cryogenic creep of copper for hundreds hours. In case blade operation at cryogenic temperatures is foreseen, the load test system used for the original creep characterization of blade material [12] could be replicated in vacuum and at cryogenic temperatures (Fig. 11).

The role of LVDTs for precision mechanical measurements and control is crucial. It is suggested to devote some runs to characterize the characteristics of LVDTs at cryogenic temperatures. Creep tests are relevant not

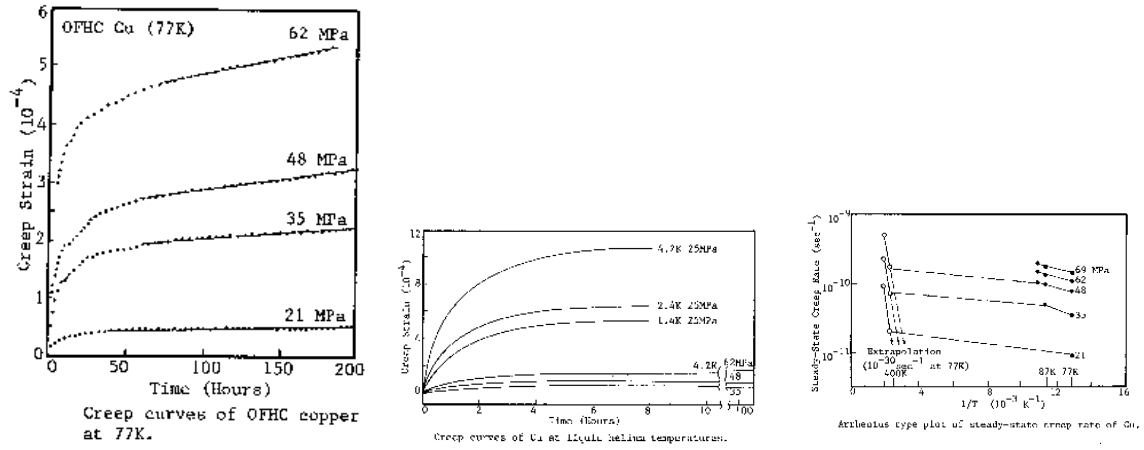

Figure 10: Creep of OFHC at 77 K (left) and 4.2 K (center); extrapolation of room temperature creep to cryogenic temperatures (right)

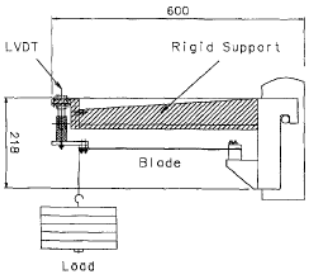

Figure 11: Setup for the blade creep measurement [12]

only for the cryogenic operation of Einstein Telescope, but also for the information they can provide about dislocations in the materials under investigation.

2.5 Mechanical studies at cryogenic temperatures

Commercial piezoelectric actuators and accelerometers for vibration studies at cryogenic temperatures are actually under investigation. Standard piezo actuators and inchworms generally have a decreased strain at low temperatures, in the range of 5 to 15 % of the total strain. Recently some new ferroelectric single crystals (PZN–PT and PMN–PT) with high strain energy density have become commercially available. The above single crystals are claimed to have strain values at cryogenic temperatures comparable to the strain of standard PZT ceramics at room temperature. Some commercial accelerometers are also available for cryogenic operation.

We are interested in measuring the quality factors of fibers at cryogenic temperatures in view of their possible use for cryogenic suspensions. The quality factor of a sapphire fiber at cryogenic temperatures has been performed by [13] using the ring down method. The apparatus is shown in Fig. 12. A piezoelectric excited the bending motion of fiber, whose oscillation was detected by a shadow meter. The whole setup was in an evacuated chamber inside a cryogenic liquid. The highest value of the quality factor was 1.1×10^7 at 199 Hz at 6 K.

The mechanical quality factor of the first two axial modes of a sapphire cylinder (60 mm length, 100 mm diameter) has been measured by [14] using the apparatus in Fig. 13. The mirror was suspended by thin sapphire fibers, with one end at 4.2 K. The approach was the ring down method: a piezoelectric excited the

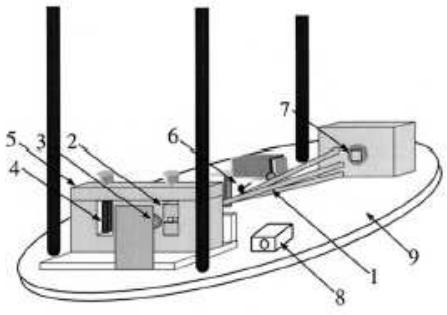

Figure 12: Apparatus used by [13] to measure the quality factor of a sapphire fiber

motion, detected by a capacitance transducer. The whole setup was in a vacuum chamber immersed in liquid helium.

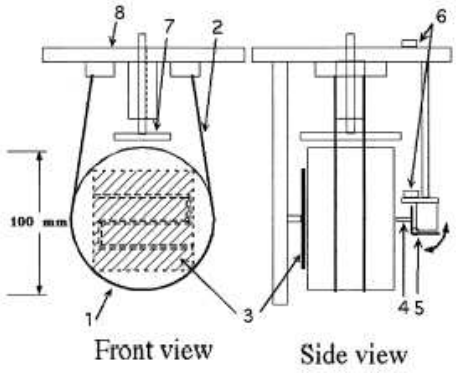

Figure 13: Apparatus used by [14] to measure the quality factor of a sapphire cylinder

The maximum value of quality factor was 2.5×10^8 at 4.2 K for the second axial symmetric mode.

The two systems can be used to characterize the quality factor of silicon fibers or silicon test masses with different characteristics.

2.6 Temperature measurement

Low temperature thermometry uses material properties with a strong dependence on temperature. The ideal thermometer should produce a minimum heat contribution in itself and in the surrounding during the measurement; it should also achieve equilibrium with a short time constant, thus it should be in good thermal contact with the probed region and should have small heat capacity. There are several primary thermometers, such as gas thermometers and thermal noise in electrical resistors, used for calibration purposes. Secondary thermometers are used in normal experimental work and calibrated against primary thermometers and/or at specific fixed points.

Resistance is perhaps the most used property for secondary thermometry, using the behavior of resistance of metals or semiconductors versus the temperature. The most common cryogenic temperature sensors [15] are resistors, either with positive temperature coefficient or negative temperature coefficient. The first class includes platinum and rhodium–iron; the second class includes semiconductors, mainly germanium.

The most used pure metal down to 10 K is platinum: the resistivity is decreasing with decreasing temperature, but below 10 K the residual resistivity becomes almost temperature independent. Platinum thermometers have

high accuracy and reproducibility. They are wire wound and suspended free of strain inside small hermetic cans. Platinum thermometers are quite bulky and consequently with slow response. They could be of limited interest in cryogenic operation of Einstein Telescope, since individual calibration is needed below 70 K. Rhodium–iron thermometers are a suitable choice when a large temperature interval must be covered by a single sensor, since they can be used up to 800 K. The physical structure of the device is identical to the platinum sensor one and it shares the same limits.

Semiconductor resistance thermometers have negative temperature coefficient, with a sensitivity increasing with decreasing temperature, according to:

$$R(T) = \alpha \exp\left(\frac{\Delta E}{2kT}\right) \tag{12}$$

where ΔE is the energy gap between the valence and conduction bands. Germanium thermometers are doped with a Ga or As doping and are considered the standard in the temperature range between 0.05 K and 100 K when no magnetic fields are present. The quoted stability is about ± 0.5 mK at liquid helium temperature. The germanium thermometers are very stable against repeated thermal cycling between room temperature and low temperature. They can be purchased with factory calibration. Typical reading currents are about a few μA at a few Kelvin. Garmanium thermometers can be a viable solution as the reference for other cheaper and more numerous thermometers in cryogenic operation of Einstein Telescope. Since the piezoelectric effect is large, the germanium part is mounted strain free inside a small hermetic can: thermal connection to environment occur only through electrical wiring, that must be thermally anchored. Self–heating of the sensor must be considered and reduced by using small excitation power.

Carbon resistors belong to the standard electronics industry and are much cheaper than germanium thermometers (at least two orders of magnitude). Thermometric properties are given by the contact resistance due to the pressing and sintering of carbon: thus there are fluctuations from sample to sample and from thermal cycling and the carbon resistors are not very reproducible. Typical commercial carbon thermometers above 1 K are 1/8 W Allen–Bradley resistors. The small typical voltages of resistance thermometers require the use of an AC bridge. Carbon resistance thermometers have widespread use due to their cheapness and the high sensitivity below a few tens Kelvin. Care must be taken to ensure thermal contact with environment, grinding away the cover. Good thermal contact is ensured by gluing the resistor inside a copper foil and sinking the lead wires to the holder. The historical Allen–Bradley resistors can be considered medium accuracy devices: periodic recalibration is necessary.

Sputtered thin films of zirconium oxynitride have good sensitivity below some tens Kelvin. The commercial brand for zirconium oxynitride is CERNOX. Bare chips are available to attain fast thermal response. Carbon–glass resistors are very sensitive below 10 K and practical down to 1 K; they share the strain free mounting of the germanium thermometers.

The forward voltage drop of a junction biased at constant current is a suitable thermometric quantity. Diode thermometers are another standard technology with high sensitivity above 1 Kelvin. The magnitude of self heating has limited the use at very low temperatures. Diodes are very reproducible within the same batch, at the level of a fraction of degree. Current noise induces reading errors and somewhat precludes high precision applications.

In the working conditions of cryogenic Einstein Telescope thermometers must cover at least the temperature range from 4.2 K to room temperature and be very small to avoid biases in measurement. The sensitivity must be high in the region of a few Kelvin, with a small error and the performances must remain stable for very long time. The response time should be small to reduce the power input for reading. The values of required sensitivity, error, stability and time response must be defined as soon as possible.

Due to the size of the Einstein Telescope system, the cost of thermometers with reproducible performances over large numbers is very important: scalability from small apparatus, where calibrated thermometers are the elective choice, is not obvious. From this point of view, cryogenic operation of Einstein Telescope shares some issues with thermometry at superconducting accelerators [16]. The request on small size, high precision, high stability and fast response probably cannot be addressed at the same time by a single thermometric technology. A selection of commercial resistors considered for a large scale application, LHC accelerator thermometry, is

shown in Fig. 14 [17]. The thermometers are CERNOX (CX), TVO ceramic resistors, rhodium–iron (RhFe) thermometers, Allen–Bradley (AB) resistors, Platinum thermometers (Pt100). The CERNOX, TVO and AB sensors have a large dynamical range and high resistance in addition to high sensitivity in our region of interest at a few Kelvin.

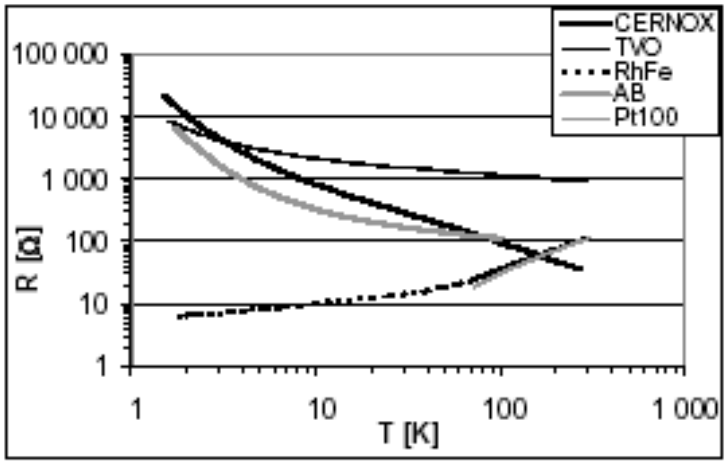

Figure 14: Behavior of resistance versus temperature for some commercial thermometers [17]

The problem of temperature monitoring in large applications has been previously addressed [18]. The cheapest but reliable technology is resistance thermometry. A careful planning is needed for mounting and heat sinking of thermometers, studying the characteristics of contact with the surface to be probed, of current leads and so on. Standardized thermometer mounting procedures must be developed. Thermometers are subject to drifts in time: the system should include periodic evaluation of characteristics with recalibration, if needed, using suitable high precision thermometers.

A starting point is the use of different thermometer technologies in the tests of thermal properties: one or more calibrated thermometers and different carbon and/or ceramic resistors and check accuracy, precision, reproducibility etc.

The cabling of thermometers must follow the same rule of standard wiring of cryostats. Since the excitation current is generally low, the electrical resistivity of wires should be low, but this implies high thermal conductance because of Wiedemann–Franz law and subsequently an high thermal load. Low thermal conductivity alloys such as phosphor bronze and manganin and, to some extent, stainless steel, can offer a right compromise between thermal conductivity and electrical resistivity. Careful heat sinking of all leads must be provided.

All suggested sensors are based on resistance: the standard read out method is the use of four wire instruments. Only diodes can be read by two wires only.

The systematic errors in resistance thermometry are due to:

- self heating of thermometer
- zero offset voltage
- ground loops
- electromagnetic pickup

The self heating of sensor is unavoidable, since power dissipation is needed to measure the resistance: there is a compromise between amount of self heating and desired precision on the temperature measurement. The zero offset voltage is the voltage measured with no current input. The effect can be removed (but not in diodes) by measuring the voltages V_+, V_- of thermometers with normal and with reverse excitation current and using

$V = (V_+ - V_-)/2$. Another solution is the use of ac excitation. The problem of ground loops is well known in all kinds of instrumentation and will not be addressed here. The electromagnetic pickup (rf noise) can be relevant for non linear detectors like diodes. The solutions are standard: use of coaxial cabling or twisted pairs and/or use of shielding.

The standard read out method of resistance thermometers is the balanced four wire ac bridge technique and suitable choice of materials for the leads, plus EMI screening. Self balancing active ac bridges are commercially available. Due to the scale of the apparatus, cryogenic operation of Einstein Telescope should develop proprietary low cost temperature monitoring and control systems, with dedicated electronics [18].

2.7 Cryogenic contamination

The lowering of temperature makes the mirrors more sensitive to contamination. The LCGT collaboration has found that the reflectance of a Fabry–Perot cavity at 10 K remained constant within 5 ppm over one month [19]. The reflectance of a Fabry–Perot cavity cooled at 10 K and exposed at a 300 K vacuum, was monitored for two months and observed to decrease by $0.12^{+0.12}_{-0.08}$ ppm per day [20]: thus a long operation time could be achieved by using a pressure level of 10^{-6} Pa in the 300 K vacuum or using tens meters of radiation shielding. The basic recipe is to start with a fully UHV compatible system at room temperature. Mirrors can be purged with thermal cycling at room temperature.

2.8 Cryostats

2.8.1 Pulse tubes

Pulse tubes offer several advantages, among them the achieving of low temperatures without liquid cryogens. Pulse tubes could potentially introduce some amount of vibration, since the cold temperature is produced by gas pressure oscillations. The LCGT collaboration has performed a study of pulse tube vibrations [21]. The vertical and horizontal spectra are shown in Fig. 15. Several resonances are evident in the cold stage spectra.

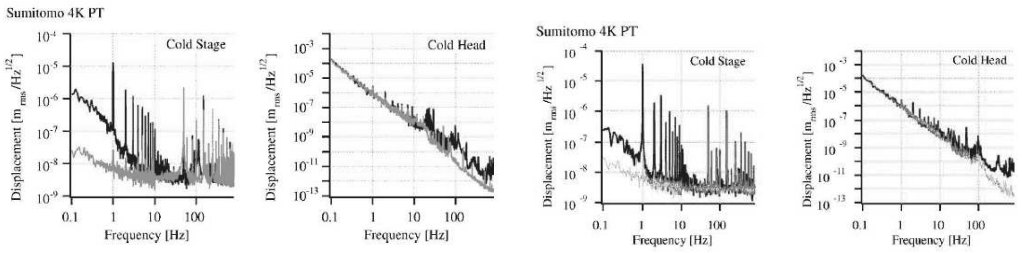

Figure 15: Spectrum of horizontal and vertical vibrations of Sumitomo 4 K pulse tube (upper curves); the lower curves are the noise of measuring system [21]

The spectra should be compared with the level of seismic noise 10^{-7} m $\mathrm{Hz}^{-\frac{1}{2}}$. The LCGT collaboration has performed further studies to deal with the 10^{-9} m $\mathrm{Hz}^{-\frac{1}{2}}$ seismic noise expected in the Kamioka mine. The vibration from the cold stage can be reduced using a flexible thermal link, made of copper blade wire or high–conductance graphite fiber thermal strap or aluminum blade wire. The LCGT collaboration has decoupled the cold head from the cryostat, using a connection with soft welded bellows and soft rubber sheets in between; in addition, a vibration isolation stage has been added in the cryostat for the cold head.

2.8.2 Dipper cryostats

Given the necessity of measuring the thermal properties of samples at different temperatures: 300 K, 77 K, 20 K, 4 K etc, it is necessary to have a test system able to cover the widest possible temperature range. The pulse

tubes suggested as the leading technology for Einstein telescope should be used for routine cryogenic testing to develop in house practice. Traditional solutions with cryogenic fluids could be useful for short tests and as a support to cryogenic pulse tube facility. Measurement at liquid nitrogen and liquid helium temperatures can be performed using an evacuated sample chamber immersed in the cryogenic liquid, taking care to provide a thermal link of samples to thermal bath.

For small samples a dipper cryostat designed for insertion into a ^{4}He storage dewar is a suitable solution [22]. The only physical constrain is the dewar neck size. These systems exhibit fast cool down time and low helium consumption, together with good temperature stability. The system described by [22] allows measurements from 300 K down to 1.3 K, with a waiting time of a few hours. Temperature is controlled with resistance heaters and measured with carbon and germanium thermometers below 30 K and platinum thermometers above. The materials are standard: AISI 304 stainless steel, brass, OFHC copper. The parts can be realized in a standard mechanical workshop.

The vacuum can is immersed in liquid helium in a storage dewar for cooling at 4.2 K: lower temperatures are achieved pumping on a pot of ^{4}He. The material is brass since it is easily machineable and cheap. The low temperature part is shown in Fig. 16, left part.

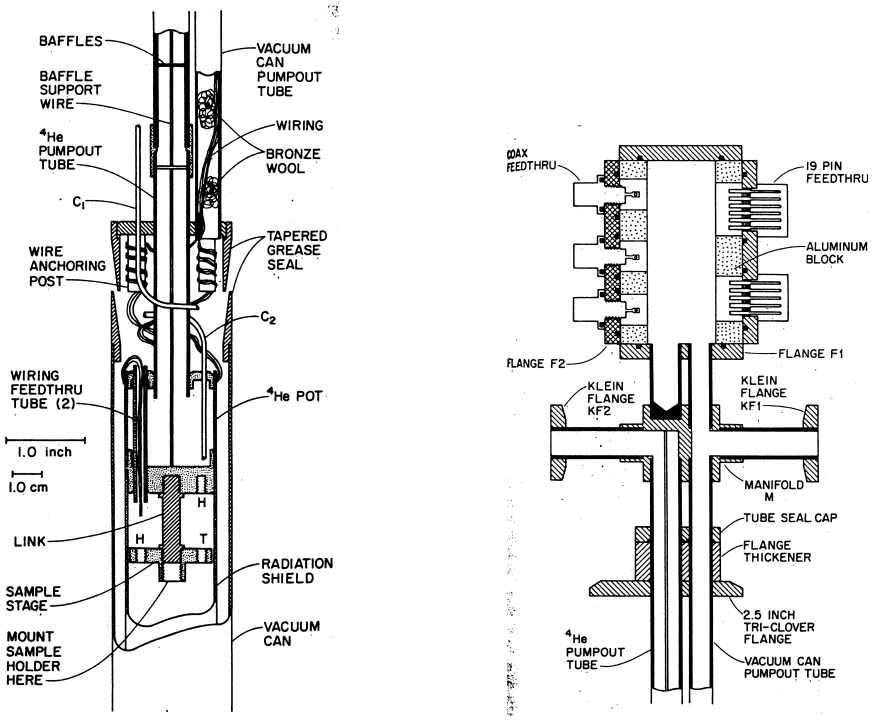

Figure 16: Left side: low temperature part of dipper cryostat by [22], where 304 stainless steel parts are solid, brass parts are crosshatched, copper parts are stippled; right side: high temperature part of dipper cryostat by [22]

The system includes two tubes, one for evacuation and another one for ^{4}He pumping. The tubes are made of 304 stainless steel, to achieve small heat capacity and low thermal conductivity, thus minimizing the heat leak. The evacuation tube contains also the electrical wiring and some bronze wool used to reduce thermal radiation load on the inner part. Inside the ^{4}He pumping tube there is a stainless steel thin wire supporting soldered copper baffles with suitable holes; the thin rod extends from the top of pumping tube to the bottom of pot. Wiring is made of constantan (for low currents) or brass (for high currents). The cabling is anchored to the suitable posts. The radiation shields and the pot are made of OFHC copper, to have high thermal conductivity and quickly achieve thermal equilibrium. Wire feedthroughs are provided for electrical connections of samples. The bottom of pot is connected to the OFHC sample stage through a brass part. The heater and the thermometers

are mounted on the stage in the positions H and T. The sample holder is made of OFHC copper and is screwed on the sample stage. It is convenient to have several holders that can be interchanged for testing. If the system is operated below 4.2 K, helium gas is filled in the pot, at beginning or continuously. Two brass capillaries C_1 and C_2 are used for this purpose; the option is not mandatory and the capillaries can be blocked with a soldered copper plug. The vacuum can needs a seal: a tapered silicon grease seal is the traditional choice for these systems, but it could be reconsidered in cryogenic operation of Einstein Telescope.

The room temperature part includes the connection to pumping and to wiring. An example with standard Klein KF flanges and standard 19 pin and coaxial connectors is shown in Fig. 16, right part. The KF_1 flange is used for vacuum can pumping, with a vacuum level of about 10^{-5} mbar; the KF_2 flange is used for the ^{4}He pump out tube. All joints must be silver soldered. The tri–clover flange seals is used on the dewar neck point and is drilled for inserting and soldering the two pumping lines.

It is suggested to cool down the dipper cryostat first at 77 K with liquid nitrogen, due to the a factor sixty between the values of latent heat of evaporation.

3 Actuators and lubrication

3.1 Motors

Some motors that are specifically designed for vacuum/cryogenic applications are commercially available.

Phytron [23] produces the VSS–Space series (Extreme Environment Stepping Motors), with the ability to work in vacuum down to 10^{-11} Torr, at temperatures from -270^{0}C to +40^{0}C. These systems are two–phase hybrid stepping motors with holding torques from 0.34 to 990 N cm, 72, 200 or 500 steps and have suitable outgassing holes to prevent pockets of trapped gases. Precision planetary gear heads are available in the catalog. In addition, K thermocouples for temperature monitoring can be added. Phytron motors have been extensively tested for space applications by several collaborations. The motors are shown in Fig. 17.

Figure 17: Phytron VSS motors [23]

MRC motors [24] are designed to work in UHV according to NASA RP–1124 specifications of TML<1%, CVCM<0.1 and, according to the factory, are able to work at liquid nitrogen and liquid helium temperature. Standard NEMA 17 and NEMA 23 parts are available. A motor is shown in Fig. 18.

Empire Magnetics [25] produces vacuum compatible motors able to operate down to low temperatures (Fig. 19). Brushless servo motors are available, with dry lubrication and chromium–nickel steel alloy components.

Maxon motors [26] have been used in the Mars rovers Spirit and Opportunity to move the six wheels, operate the cameras and move the robotic arm. Each rover is equipped with 39 Maxon DC motors (Fig. 20), able to withstand temperature variations that range from -120^{0}C to +25^{0}C.

Donovan Micro–Tek motors [27] have been used by NASA in satellite applications. Precision miniature stepper motors with MoS_2 bearing lubricant were tested immersed in liquid nitrogen and liquid helium. In addition they have also been tested in a vacuum better than 10^{-5} mbar with temperatures between 4 K and 300 K. The

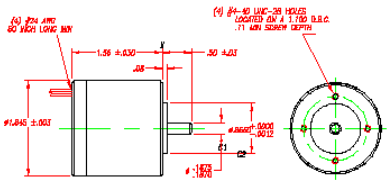

Figure 18: MRC motor [24]

Figure 19: Empire Magnetics motor [25]

Figure 20: Maxon DC motors [26]

motors have a 15^0 step angle and can be full, half–stepped or micro–stepped. Nominal holding torque is .84 ounce–inches with two phases on.

Figure 21: Donovan Micro–Tek motor [27]

Commercial piezoelectric motors for cryogenic and UHV use are produced by New Scale Technology [28]: the travel is up to 50 mm, with 20 nm resolution and the system holds position with power off. A motor belonging to SQUIGGLE series is shown in Fig. 22. The motor is guaranteed to operate continuously from room temperature to liquid helium temperature and has been tested at NASA facilities.

Figure 22: Cryogenic SQUIGGLE motor [28]

The standard piezo ceramics exhibit a very reduced strain (5% to 15%) at cryogenic temperatures. The single crystal piezoelectric material developed by TRS is an exception, since the strain at cryogenic temperatures is similar to the strain of standard piezo materials at room temperatures. The TRS ceramic single crystal actuators have been tested at 77 K. The achieved performances were a stroke above 10 mm, a step resolution of about 20 nm at a driving voltage of some tens Volts peak to peak. The possibility of studying the behavior at lower temperature should be considered.

Superconducting film actuators have been investigated by the Japanese collaboration [29] as a possible replacement of solenoid coils and permanent magnets used for test mass actuation. The investigated cryogenic actuator operates at 77 K and has a superconducting YBCO film with 1.6 μm thickness glued to the test mass driven by a coil. The selection of superconducting material was driven by the necessity of operating above 20 K in the final setup. A force of up to 0.2 mN could be applied (Fig. 23), with a goal of 2 mN for the LCGT test mass actuation.

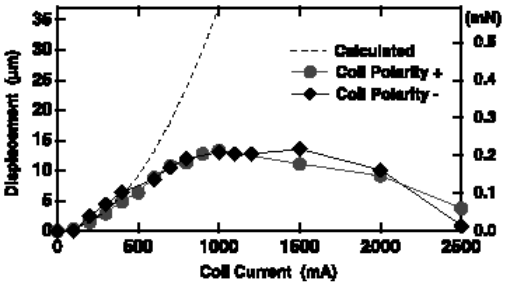

Figure 23: Force of the YBCO actuator as a function of coil current (right scale) [29]

Recently, a stepping motor by AML [30] has been successfully operated down to a few Kelvin in the context of the ILIAS initiative.

3.2 Cryogenic lubrication

Cryogenic actuators need special lubrication to ensure a low friction for a long operation time. Space missions have sometimes used liquid lubricants based on mineral oils, typically mixtures of hydrocarbons, such as Apiezon

C. Their use in Einstein Telescope is not recommended because of contamination concerns. Perfluoropolyethers (PFPE), such as Fomblin or Krytox, are based on fluorine and could also be a concern from the contamination point of view. However, the main drawback of liquid lubricants is the much larger volatility compared to solid lubricants. Only solid lubrication can be considered at cryogenic temperatures. In cryogenic operation of Einstein Telescope lubrication will be used for motions and adjustments, but as one shot and not cyclical operation. The mechanisms will operate seldom and at low speed, with long quiescence intervals before use, but permanently inside a cryogenic UHV environment. Actuators do not undergo many duty cycles, but they put strong stresses on the lubricant with intervals with long quiescence times. Solid lubricants are the suitable choice, since the stay in the contact region and offer low friction coefficients.

The lubrication issues have been explored by NASA and ESA for space applications. The possible lubricating materials are polymers, soft solids, lamellar solids. Polymeric materials include polyimides and polytetrafluoroethylene: they can be of concern in cryogenic operation of Einstein Telescope because of contamination. Soft solids for lubrication include lead and silver. Ion plated lead has been used together with leaded bronze cages in cryogenic vacuum for small loads and low speeds. The lifetime in air is quite short due to oxidation and fast wear. Lead and bronze can be of concern in cryogenic operation of Einstein Telescope because of contamination. Lamellar solids include molybdenum disulphide (MoS_2) and tungsten disulphide (WS_2), well known for their widespread use in UHV lubrication. Lamellar solids and soft metals are applied using ion plating or sputtering techniques. MoS_2 is usually applied by sputtering. It is an hygroscopic material and moisture should be avoided. Dicronite lubrication [31] uses DL–5, a modified WS_2. The surface of application is treated to achieve a structure free of impurities and oxides and the tungsten disulphide becomes part of the support. The typical thickness is below 0.5 microns. Dicronite has been successfully used from about 800 K down to liquid nitrogen temperature. It is stable down to a vacuum level of 10^{-14} torr. Diamond–like–carbon (DLC) is a recent entry in solid lubrication which is being investigated for space applications.

Some commercial solutions for bearings are available. The balls and roller bearings by RBC [32] (Fig. 24) are made of AISI–440–C, with a preliminary treatment at liquid nitrogen temperature to achieve the dimensional stability required for cryogenic operation. The bearing separators are made of fiberglass reinforced Teflon. Teflon and organic materials should be screened for contamination if use in cryogenic operation of Einstein Telescope is foreseen.

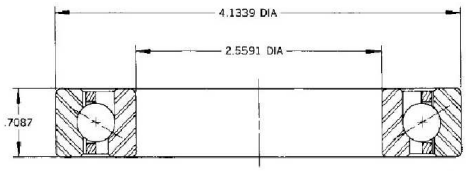

Figure 24: RBC cryogenic bearing

Another cryogenic combination for ball bearings includes stainless steel rings and ceramic balls. RMB [33] produces bearings that has been widely used in cryogenic applications. ESTL [34] provides differential solutions for bearings and lubrication for space applications.

3.3 Conclusions

Some commercial solutions for actuators and lubrication at cryogenic temperatures are available. It is suggested to qualify motors in the operating conditions of Einstein Telescope.

4 Cabling

The large number of sensing and control systems in cryogenic operation of Einstein Telescope will require thousands electrical connections, involving sensing wires with negligible current, but also coils and actuators with high current and larger heat load. An excessive thermal load can lead to high wire temperatures and risk of insulation damage.

Electrical connections must fulfill the standard mechanical and vacuum requirements of Einstein Telescope:

- high flexibility
- low hydrocarbon contamination

But also:

- low thermal conductivity, to reduce heat budget from external environment
- low electrical resistivity, to reduce heat injection via Joule heating
- capability to resist to large thermal contractions
- ability to operate for years at temperatures as low as 4 K, with thermal cycling

Addressing the cabling in cryogenic operation of Einstein Telescope will require a detailed study to define several parameters: definition of electrical connections (signal cabling, power cabling etc); electrical parameters; maximum allowed thermal dissipation; mechanical stiffness; maximum allowed contamination.

4.1 Some guidelines for design

We will focus on the thermal and electrical constrains on cryogenic leads cooled by conduction. For sake of simplicity, we will consider an homogeneous wire with constant cross sectional area A and length L, resistivity $\rho(T)$, thermal conductivity $k(T)$, where T is the temperature, assumed to be a function of axial position only. The axial position x is measured starting from the cold end. We will assume that the wire ends are at temperatures T_L and T_H, with $T_L < T_H$. The wire current is I.

Heat budget due to thermal conductivity is proportional to the cross section and inversely proportional to the length, favoring long thin wires with low thermal conductivity. There will be also an ohmic contribution due to Joule heating. For this process, heat budget is reduced by choosing thick and short wires with low electrical resistivity.

The steady energy balance equation for conduction cooled leads is:

$$\frac{d}{dx}\left(kA\frac{dT}{dx}\right) + \rho\frac{I^2}{A} = 0 \tag{13}$$

with the boundary conditions $T(0) = T_L$, $T(L) = T_H$.

The heat Q_L at $x = 0$ will be:

$$Q_L = \sqrt{Q_H^2 + I^2 \int_{T_L}^{T_H} 2\rho(T)k(T)dT} \tag{14}$$

where Q_H is the heat at $x = L$. The quantity is minimized when $Q_H = 0$:

$$Q_L^{minimum} = I\sqrt{\int_{T_L}^{T_H} 2\rho(T)k(T)dT} \tag{15}$$

The optimal wire dimension is given by:

$$\frac{L}{A} = \int_{T_L}^{T_H} \frac{k(T)dT}{\sqrt{Q_H^2 + I^2 \int_T^{T_H} 2\rho(\tau)k(\tau)d\tau}} \tag{16}$$

In the special case $Q_H = 0$ the expression becomes:

$$\frac{L}{A}(Q_H = 0) = \frac{1}{I} \int_{T_L}^{T_H} \frac{k(T)dT}{\sqrt{\int_T^{T_H} 2\rho(\tau)k(\tau)d\tau}} \tag{17}$$

The optimal dimension depends not only on material properties, but also on the current, the end temperatures and Q_H. Optimization is achieved for a single operating current, with $Q_L^{minimum} \propto I$ and $L/A \propto I^{-1}$.

For insulated wires, coaxial cables and ribbons heat conduction occurs not only through conductors, but also through insulation. On the other hand, Joule heating occurs at the conductor only. Thus the combination of conductor and insulant must be optimized. We will now discuss some issues about conductor and insulation materials.

The thermal conductivity of several materials is summarized in Fig. 1 for reference.

4.2 Conductor materials

The requirements of low thermal conductivity to reduce external heat injection and of low electrical resistivity to reduce Joule heating are in contrast. The electrical resistivity of metals decreases by two orders of magnitude from room temperature to 4.2 K; the thermal conductivity has a maximum at one twentieth of the Debye temperature and a linear decrease below. The electrical resistivity of alloys is weakly decreasing from room temperature to a few Kelvin, while thermal conductivity decreases by one or two orders of magnitude.

The standard conductor materials for cryogenic operation are: stainless steel, constantan, manganin, brass, copper.

The thermal conductivity of copper and stainless steel is detailed in Fig. 25, left and right.

The electrical resistivity of brass, constantan, manganin at 295 and 4.2 K is summarized in Table 1.

Material	$\rho(\mu\Omega\cdot$ cm) at 295 K	ρ ($\mu\Omega\cdot$cm) at 4.2 K
Brass	7	4
Constantan	52.5	44
Manganin	48	43

Table 1: Resistivity of brass, constantan and manganin at 295 and 4.2 K [2]

The resistivity of copper (strongly dependent on the purity grade) and stainless steel is shown in Fig. 26.

Constantan and manganin are good choices for signal wires because of their low thermal conductivity and the weak dependence of electrical resistivity on temperature. Compared to constantan, manganin offers higher electrical conductivity, but also higher thermal conductivity. For large currents, copper is sometimes preferred because of its better electrical conductivity, despite its high thermal conductivity: large diameters to reduce Joule heating and some intermediate heat sinking are required.

4.3 Insulation materials

The main challenge of insulation at cryogenic temperatures, in addition to the standard requirements of electrical insulation, is the resistance to mechanical stresses induced by thermal contraction and thermal cycling during

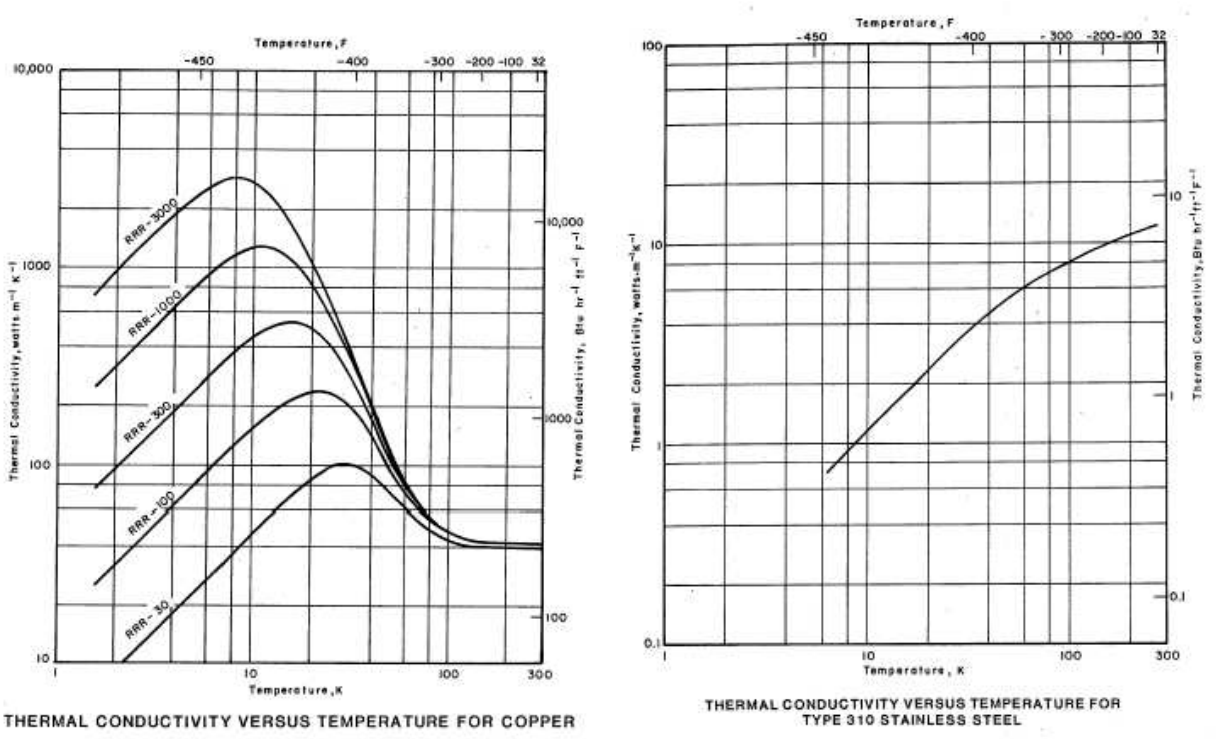

Figure 25: Thermal conductivity of copper and stainless steel [35]

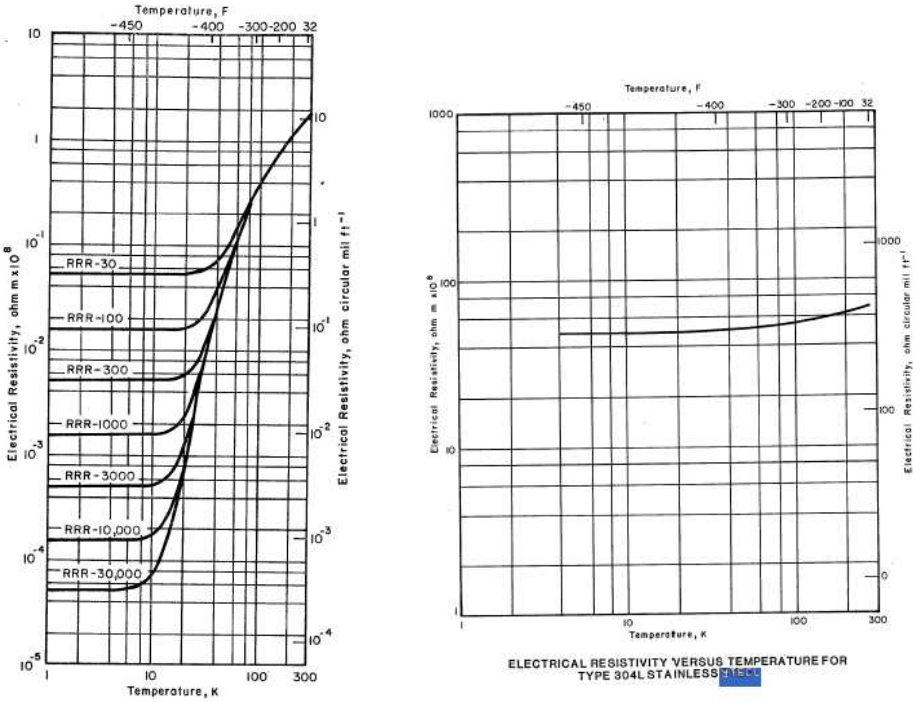

Figure 26: Electrical resistivity of copper and stainless steel at cryogenic temperatures [35]

operation. The intrinsic mechanical stress can lead to faults. The standard shock test before operation is performed by immersion in liquid nitrogen.

Some low outgassing samples that are quoted to be usable at low temperatures have been studied in the context of Virgo investigations about contamination:

- wires with Pyre–ML insulation [36]; Pyre–ML is a Dupont aromatic polyimide that can undergo also high temperature baking
- ribbons with Gore–Tex insulation [37]; Gore–Tex is an expanded polytetrafluoroethylene
- alumina insulated wires [38]

Some of them could be used for coils or signal connections. Kapton, a traditional choice for ultra high vacuum cabling, is also a standard for cryogenic insulation. Pyre–ML is very similar to Kapton, from the point of view of thermal and mechanical properties. The Virgo contamination measurements have found that Kapton nominal insulation is often not pure Kapton. Kapton insulated cables have shown emission by FEP layers [39]. Kapton ribbons from different manufacturers have shown emission by adhesives used to seal the various layers [40], [41]. The additional components were not observed in the emission of Pyre–ML. As a reference, the thermal conductivity of Kapton tape between 5 and 300 K is $5.24\times10^{-3}\ T^{1.02}$ W m^{-1} K^{-1} [42], see Fig. 27, a).

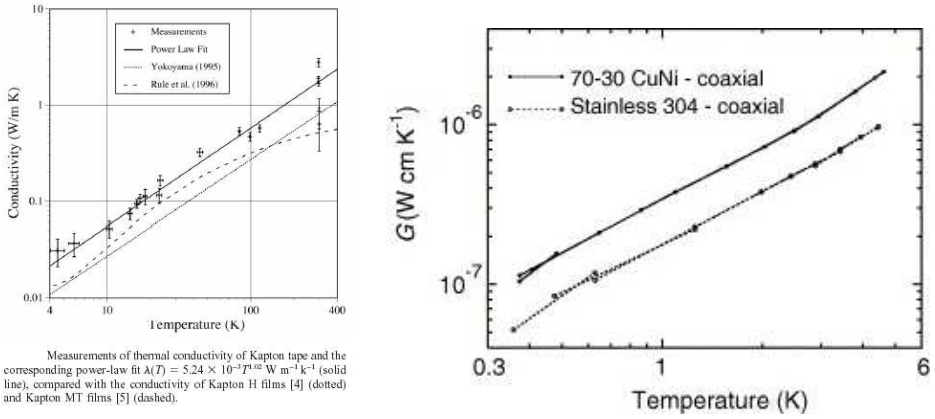

Figure 27: a) Thermal conductivity of Kapton tape at cryogenic temperatures [42]; b) Coax Co., LTD: thermal conductivity of miniature coaxial cables [43]

From the point of view of thermal and mechanical properties, but not from the point of view of outgassing, Gore–Tex is very similar to Teflon, whose thermal conductivity is shown in Fig. 1). Coax Co., LTD, produces semi-rigid cables for low temperature operations, with different conductors: stainless steel (SUS304), Cupronickel, Niobium, Oxygen-free copper and silver. The thermal conduction between 0.3 and 4.5 K of miniature coaxial cables (cross section 8.6×10^{-4}cm^2) by Coax Co., LTD, has been measured by [43]. The cables were made of 70-30 CuNi and stainless steel 304, with PTFE insulation (Fig. 27, b)). The low temperature properties of Gore–Tex in the form of woven fabric has been investigated in [44], where it was shown that it is a strong and flexible material at low temperatures. The Planck IR telescope collaboration has recently considered ribbons with flat conductors on Kapton and on Gore–Tex to replace the traditional cryogenic coaxial cables with stainless steel conductors [45].

4.4 Commercial solutions

Flexible ribbons able to work down to 0.5 K are commercially available. The typical insulation is Kapton, with several choices for conductors (manganin, copper, constantan, stainless steel, brass). An example are the ribbons developed for the Herschel mission, with Kapton insulation and brass or steel conductors.

Caburn offers stainless steel cryogenic instrumentation wires with Kapton type F insulation for use down to liquid helium temperature (Fig. 28).

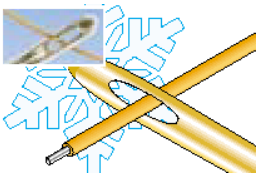

Figure 28: Caburn: cryogenic wire

Tayco Engineering offers some products that can be used down to liquid nitrogen or liquid helium temperatures. The ultra miniature ribbon cable provides high flexibility at low temperatures (Fig. 29, left). The ribbon includes 9 gold plated nickel conductors and an outer thin gold layer for shielding. The ribbon is very light and can be baked up to 200 ^{0}C. It is used for interconnection of detectors on satellites and has been qualified for Mars missions and others. The same factory offers also a cryogenic shielded twisted pair ribbon cable (Fig. 29, center), with 24 twisted pairs of 40 AWG manganin wire and vacuum deposited aluminium shielding. This product has been used for instrumentation of Cryogenic Telescope Assembly (CTA) and is NASA Space Flight Qualified. The cryogenic focal plane ribbon cable (Fig. 29, right) is available with straight or twisted conductors and has been qualified for NASA Space Infrared Telescope Facility (SIRTF), Mars Missions, MAP and other missions.

Figure 29: Tayco Engineering: ultra miniature ribbon cable (left); shielded twisted pair ribbon cable (center); focal plane ribbon cable (right)

STAR Cryoelectronics provides wires and cables with copper, phosphor–bronze, niobium conductors and Poly–Nylon, Formvar insulation and flexible cryocables (Fig. 30), with braided stainless steel shield and 10 or 14 pin LEMO end connectors. The CBL–C2 cryocable standard wiring includes multiple twisted pairs of phosphor–bronze or copper wire with polyimide insulation. The warm side connector is vacuum sealed.

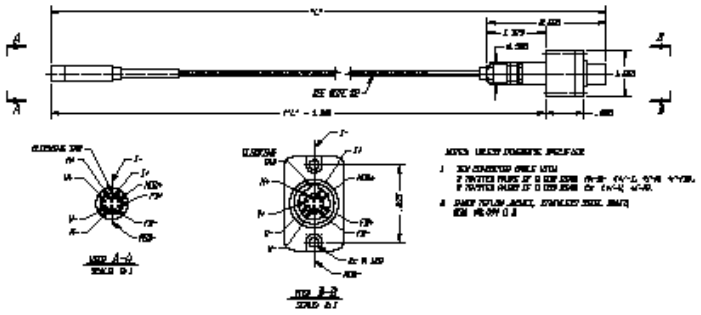

Figure 30: Star Cryoelectronics: CBL–C2 cryocable

Oxford Instruments offers sub–miniature coaxial cables (Fig. 31, left), with conductor and shields made of stainless steel or copper and Teflon insulation. Cryogenic ribbon cables are available (Fig. 31, center), with twisted pairs of constantan wires and polyester insulation. Ribbons are available without or with connectors. In the last case, the low temperature MDM connectors (Fig. 31, right) are potted to the cable.

Figure 31: Oxford Instruments: a) stainless steel coaxial cable; b) ribbon cable; c) MDM metal connectors

Lake Shore offers phosphor–bronze cryogenic wire with Formvar or polyimide insulation, twisted pairs (phosphor–bronze with polyimide insulation) and ultra miniature coaxial cables (Fig. 32), with copper or 304 stainless steels conductors.

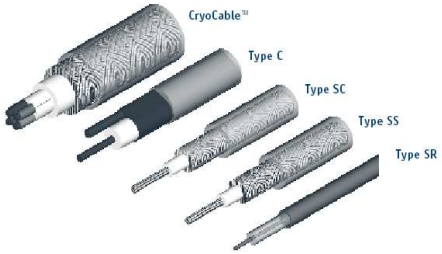

Figure 32: Lake Shore coaxial cables

4.5 Conclusions

Different solutions are potentially available for cabling of cryogenic Einstein Telescope. It is suggested to dimension the power and signal cabling, including the heat transported by conduction and the heat produced by Joule dissipation.

5 Adhesives

Adhesives to bond different components will be needed in several parts of cryogenic operation of Einstein Telescope, in particular for the antisprings and the mirror magnets. The adhesives used in cryogenic environments must provide enough strength to bond materials to each other, but also to sustain thermal cycling. The different thermal expansion coefficients of adhesive and bonded components can produce large mechanical stresses and failure of bonding. The adhesion itself depends on several factors, including the characteristics of surfaces to be bonded. Highly polished optical surfaces offer a smaller contact area than rough surfaces and in principle lead to weaker bonds. When bonding magnets to supports, the bonding is intrinsically stronger on the magnet side because of its porosity.

The aim of this note is a preliminary literature survey of adhesives reported to be serviceable at cryogenic temperatures, as a starting point for possible testing. Published data of cryogenic adhesives are still scarce and extrapolations of room temperature measurements are not necessarily valid. Moreover, the performances

depend on the production batch and on the preparation and curing procedures. Several targeted investigations will be necessary.

The use of adhesives in cryogenic operation of Einstein Telescope involves several aspects that will need a quantitative definition in view of the long foreseen operation:

- strength of adhesive bond for each application
- adhesive capability to sustain thermal cycling
- differential thermal expansion coefficient of materials to be bonded
- maximum level of tolerable contamination
- aging of adhesive
- for magnet–mirror systems: impact on the quality factor of mirror

Some choices could have an impact on design. For example, it could be necessary to find particular combinations of adhesives and support materials to reduce differential thermal expansion stresses.

For the scope of the present discussion, the adhesives will be divided into two broad classes: epoxies and inorganic adhesives. A preliminary description of adhesives claimed to be usable at cryogenic temperatures will be firstly given. Then published measurements of epoxy properties (bonding strength, thermal expansion coefficient, thermal conductivity) will be summarized.

5.1 Adhesives

The historical workhorses for cryogenic bonding are the two epoxies Stycast 1266 and Stycast 2850 FT [46]. Both of them show good bonding to metals, but poorer bonding to optical surfaces. Stycast 1266 [47] is prepared by mixing two basic components: since the reaction is exothermic, the preparation is limited to small batches. Stycast 1266 is a transparent compound that easily bonds to metals. Before curing, it has such a low viscosity that can fill small holes and tubes, being able to act also as a sealant. After curing, it can be machined to the desired shape. The thermal expansion coefficient is quite large (of the order of 1% at liquid helium temperature) and must be taken into account in the design stage. Stycast 2850 FT [47] is a black resin loaded with metal powder to match the thermal expansion coefficient of metals. The adhesion to metals is quite good, but the compound is not easily machinable. Stycast 2850FT has been selected, in the context of cryogenic interferometers, by the LCGT collaboration [48]. An actuator made of a superconducting film and a solenoid coil was used to exert a force on a test mass. Other epoxies are quite similar to the Stycast series. Eccobond 285 [47] is a thermally conductive epoxy paste adhesive designed for bonding ceramic and metals to heat sinks, quite similar to Stycast 2850 FT. Poxycomet F is another epoxy loaded with aluminum useful for aluminum bonding [49]. The three epoxies Stycast 2850 FT, Eccobond 285, Poxycomet F are advantageous from the point of view of mechanical performance, but not for electrical insulation.

CryoBond adhesives [50] are claimed to have good adhesion and sealing properties at cryogenic temperatures. They are used to seal dewars and to bond sensors, strain gauges and superconducting elements. Other applications are coating of leads and magnets and joining of piping that cannot be welded or brazed. Cryobond 620 is a low viscosity epoxy for substrates that must undergo thermal cycling. It can also be used as a leak stop for cryogenic piping. Cryobond 621 is loaded with fillers and has similar properties. Cryobond 920 is a two part solvent free epoxy that can work at cryogenic and at high temperatures. It is a high strain adhesive with small hollow microspheres as insulators.

Master Bond [51] offers some epoxies with low outgassing (according to ASTM E–595 standard) for use at cryogenic temperature, down to 4 K: EP21TCHT-1 (thermally conductive), EP21TDC-2, EP21TDCS, EP29LPSP, EP30FL, EP37-3FLFAO, EP51M, Supreme 10HT and 10HTS. Supreme 11F is usable down to 200 K.

Armstrong A-12 [52] is a general purpose epoxy claimed to withstand cryogenic temperatures. The epoxy has a non critical mixing ratio that is tuned according to the required bond flexibility.

PR-1665 by De Soto [53] is a potting and moulding compound (based on polyurethane) with high tear and tensile strength. It is serviceable down to 77 K.

3M Scotch–Weld Epoxy Adhesive 2216 B/A [54] is considered excellent for cryogenic bonding applications. Overlap shear test have been performed down to 20 K. DP 190 [54] offers high electrical insulation at the level of some tens kV/mm. It is a version of 3M 2216 B/A with 1:1 mixing.

Hysol EA 9361 [49] is a high elongation paste adhesive that has been tested down to 77 K.

At the interface between adhesives and sealant we mention the compound based on silicone resin described by [55], vacuum tight down to 4 K.

The epoxies are intrinsically subjected to air trapping during component mixing and they must be pumped during curing inside a vacuum vessel, to extract bubbles. Compounds based on silicone and organic compounds deserve a special contamination investigation.

Inorganic adhesives are based on alumina, zircon, magnesia etc and are marketed as high temperature adhesives, able to withstand temperatures up to 1000 or 2000 K. However, some of them are claimed to be serviceable down to a few Kelvin. Being inorganic, the problem of contamination is potentially reduced compared to epoxies, if the adhesives are properly prepared and handled.

Resbond ceramic adhesives [56], designed for use up to 1000 K, are based on alumina, zirconium, zircon, mica, magnesia, silica or graphite. Resbond 919 is based on MgO, zirconia and water. Resbond 903 is a pasty alumina and can be used down to 200 K. Resbond 940 is based on zircon powder with liquid activator and is used to encapsulate heaters and high temperature sensors. Resbond 907 is based on mica and is serviceable down to about 90 K. Resbond 907GF has been used to glue titanium foils down to 88 K [57]. Thermeez 7030 is a SiO_2 based adhesive ([56]).

Aremco high temperature adhesives [58] are based on alumina, alumina-silica, silica, graphite, zirconia, magnesium oxide, boron nitride and aluminum nitride. Two of them, Aremco 571 (magnesium oxide) [59] and Aremco 538 [60], have been tested in the context of the Virgo outgassing tests. An example of cryogenic application of Aremco 571 down to 110 K is described by [61].

Sauereisen chemical set cements [62] are used for potting and bonding. Low Expansion Cement No. 29 is an inorganic cement loaded with zircon used to embed heaters, thermocouples, resistors and coil coating. It is claimed to be strongly resistant to cryogenic conditions. Plastic porcelain No. 30 is based on magnesium oxide and is used for wire insulation and to fill hollow cavities. It slight expands during hardening. The compound is stable down to 200 K.

5.2 Suggested investigations

We suggest to perform studies of bonding strength, thermal expansion coefficient, thermal conductivity, contamination and aging. In the following some investigations reported in literature will be presented.

5.2.1 Bonding strength

A detailed investigation of bonding to polished optical surfaces down to 4.2 K has been performed by [63].

The standard tests of bonding strength are the Scotch tape test and the razor blade test. In the former test the tape is attached to the adhesive and pulled to check whether the adhesive is detaching. In the latter test a razor blade is used to try lifting the adhesive surface. Such tests do not produce quantitative estimations. Moreover, the razor test is of great concern for the safety of Einstein Telescope mirrors.

The work by [63] investigated the bonding of several adhesives to glass samples. Adhesives were cured at temperatures up to 150 ^{0}C. The thermal cycling between room temperature and 4.2 K was simulated by cycling between room temperature and 77 K, since most of thermal contraction occurs between room temperature and

liquid nitrogen temperature. The polished optical surfaces used for tests were microscope slides. A piece of paper with a round hole was positioned on the bottom slide. The hole was then filled with adhesive and another slide was pressed from top. The bond strength was qualified by the adhesive release force per unit area (ARFA) $\sigma = \frac{F}{\pi R^2}$, where F is the applied force and R the radius of the adhesive circle. The force was produced by a weight hanging with a lever arm . The explored ARFA interval ranged from 1 to 10, with ARFA in units of 3.0×10^5 kgf/m^2.

For a first set of tests the epoxies were cured at 50–75 ^{0}C, but not degassed, and tested down to liquid nitrogen temperature. The results are summarized in Fig. 33. Some adhesives included in the table are not specifically addressed for low temperature use, being nominally usable down to -60 ^{0}C at most. The Devcon and Loctite adhesives are not designed for cryogenic use. Torr–Seal is designed for use between -45 and 120 ^{0}C. Permabond epoxy is serviceable between -55 and 80 ^{0}C. The epoxy Lord 305 has a nominal operation temperature between -34 and 121 ^{0}C. Stycast 1266 and 2850FT showed poor bonding to glass. Silicone rubber showed internal fracture. The 5 minute epoxy showed intermediate performances, since it underwent internal rupture and was weakened by thermal cycling. The optically clear adhesive 8141 showed weak bonding properties. Armstrong A–12 prepared in the 1:4 mixing ratio suggested for cryogenic operation (because of increased flexibility) bonded worse than the 1:1 mixing version and was too weak at room temperature. Dow Primacor 3460 (ethylene copolymer) bonding strength was satisfactory and improved with increasing temperature. Hercules furnace cement released with small applied force, but taking away glass pieces. Lord 305 showed a good performance quite independent on the mixing ratio. It was successfully tested as a sealant for feed–throughs, windows and tubes and selected for further testing at 4.2 K because of its good performances. It was outgassed by heating at 40 ^{0} C and pumped to remove bubbles. The performances were good and showed that Lord 305 could be used for cryogenic sealing also. During the first phase of testing, some aged epoxies were investigated. Generally, aged epoxies performed more poorly than freshly prepared ones. Variations among the same adhesive were also observed.

A second set of tests was performed with the epoxies Master Bond Supreme 10HT ND2, Miller Stevens 907 epoxy, Lord 305, Stycast 1266 and 2850 GT, to investigate the effect of curing temperature and time. The bonding strength of the last three epoxies improved with high temperature (60 or 100 ^{0}C) curing and preliminary degassing of epoxy. High temperature cements were also studied: Omega CC, Resbond 903, Resbond 940, Resbond 919, Thermeez 7030. The first one, not described above, is made of zirconium silicate and sodium silicate binder. Cements failed from the cohesive point of view, but strongly adhered to glass.

As a general trend, variability was observed for the same adhesive from batch to batch and aged epoxies performed poorly compared to freshly prepared ones. Bonding strength improved with preliminary degassing and curing temperature and interval must be tuned. However, adhesives suitable for optical surfaces should perform better with rough surfaces.

The KIRMOS (Keck near Infrared Multi Object Spectrograph) collaboration has tackled the problem of bonding fused silica, sapphire, CaF_2 and zinc selenide lenses to metal mounting blocks in a system that must undergo thermal cycling [64], [65]. Only the reports about the first three materials, of interest for cryogenic operation of Einstein Telescope, will be summarized here. The first tests have been performed on lenses glued to copper beryllium tabs and cooled down to 100 K [64]. The selected adhesives for the first runs were Loctite Aerospace Hysol EA 9313 and Tra–Con Supertherm 816H01. Bonding of CaF_2 to both adhesives was satisfactory, since the thermal expansion coefficients of copper beryllium and CaF_2 are very similar. Bonding of Hysol EA 9313 to silica was poor, with some episodes of breaking with moderate handling. The bond broke inside silica itself, suggesting that integrity was compromised because of differential contraction. Bonding of Supertherm 816H01 was poor, since cleavage occurred into adhesive itself. Sapphire showed poor bonding to both adhesives, that detached from the clean surface. In a second run [65] the metals of mounting blocks was chosen to match the thermal expansion coefficient of lens material. Fused silica was bonded to the iron–nickel alloy AL 36, sapphire to tungsten alloy, CaF_2 to 304 stainless steel. All samples underwent cooling and pull tests at 150 K and room temperature. The selected adhesives were Epibond 1210A/9615A, Armstrong A–31, Aremco Bond 556, Masterbond EP2TCHT–2, Duralco 4538, Stycast 2850 FT. The best performances were achieved by Epibond 1210A/9615A and Armstrong A–31. They formed a bond much stronger than substrate itself: the pull–off operation extracted chunks of fused silica substrate and cracked the CaF_2. Sapphire bonding was satisfactory,

TABLE I. The numbers in the columns give the (quantized) weight for release. For example, the number 2 means release occurred when the second weight was placed in the weight pan; there is no zero on this scale. Numbers in parentheses are the number of tests with a given value carried out on this adhesive. Emerson & Cuming 1266 and 2850-FT are known to thermally cycle well, so thermal cycle tests were not conducted.

Material	ARFA (3×10^5kgf/m^2)	ARFA (cycled to 77 K)	Comments
Emerson & Cuming 1266 epoxy	1(2); 2(1); 3(1)		
Emerson & Cuming 2850 FT epoxy	1(2); 2(2); 3(5)		
Devcon DA120 epoxy	1(1)		
Devcon Epoxy-Plus	3(1)	2(1)	
Devcon 5 minute epoxy	5(1); 4(1)	1(1)	Internal fracture
Varian Torr-Seal epoxy	6(1); 3(2)	6(1)	
APS A-4000 epoxy	3(1)		
Lord 305 epoxy	4(5); 7(1) 8(1); 9+(1)	4(1); 7(1)	Internal fracture for lower values; for 9+ slide broke
Armstrong A-12, 1:1	2(1)	2(1)	
Armstrong A-12, 1:4	1(2)		Tacky after cure, internal fracture
Permabond E-32 epoxy	3(1); 2(1)	5(1); 3(1)	Internal fracture
3M-8 epoxy	2(1); 5(1)	4(1)	
3M-9 epoxy	4(1)	2(1)	Surface release and internal fracture
8141 Optical Clear Adhesive	1(5)		
Epotecny E-505 epoxy	1(4)		
MS 907	3(1); 4(4); 5(1)	4(3)	
Loctite E-120P	1(3); 2(1)		
Loctite E-30CL	3(4); 4(1); 5(1)	1(1); 3(2); 5(1)	
Chemlok 134	1(2)		Released with handling
Cyanolit 203	2(1)		
Dow Primacor 3460	6(2); 7(1)	6(1)	
GE RTV 108 Silicone	1(3)		Internal fracture
Aquarium sealant	1(2)		Internal fracture
Hercules furnace cement,	1(2)		Strong adhesion; see the text
Resbond 903, 940, 919, and Thermeeze 7030	1-2		Strong adhesion, see the text

Figure 33: Performances of different epoxies [63]

improving at lower temperatures. It was observed that Epibond 1210A/9615A showed gravity induced flow during setting.

The bonding of silicon to a substrate has been addressed by [66] in the context of the SNAP mission CCD, that must operate at 130 K in space. The Young modulus and the Poisson ratio have been measured at 295, 250, 200, 150, 100 K for the epoxies Hysol 9361, Tra-Con F113, Epotek 301-2. Tra-Con F113 is designed for use between -60 and 100 ^{0}C. The results of the tensile tests are summarized in Fig. 34 for room temperature and 100 K.

An investigation centered on the properties of the surfaces to be bonded has been performed by [67], studying the adhesion of CTD-101K [50] to Incoloy 908. The shear strength at liquid nitrogen temperature was better by 40% than that at room temperature. Acid etching and water rinse for surface preparation created a high bond strength.

Some adhesives for LHC magnet collars have been tested by [68] at 1.8 K and in a radiation environment. The selected adhesives, tested with stainless steel and 5083 aluminum alloys, were Araldites AZ 15/HZ 15, XD 4447/4448, AW 106/HV 953 and Stycast 2850 FT. The test procedure included 5 minutes in liquid nitrogen

Ambient

Tra-Con F113	Elastic Modulus (psi)	356886± 12523	3.51%
	Poisson's Ratio	0.401±0.003	0.64%
	Maximum Stress (psi)	2539± 86	3.40%
Epotek 301-2	Elastic Modulus (psi)	531427± 6166	1.16%
	Poisson's Ratio	0.358±0.001	0.35%
	Maximum Stress (psi)	3751± 45	1.21%
Hysol 9361	Elastic Modulus (psi)	154678± 1526	0.99%
	Poisson's Ratio	0.433±0.007	1.67%
	Maximum Stress (psi)	1153± 9	0.77%

100 K

Tra-Con F113	Elastic Modulus (psi)	1105895± 40675	3.69%
	Poisson's Ratio	0.348 ± 0.005	1.44%
	Maximum Stress (psi)	7092± 649	9.15%
Epotek 301-2	Elastic Modulus (psi)	1014310± 14384	1.42%
	Poisson's Ratio	0.350 ± 0.008	2.34%
	Maximum Stress (psi)	6783± 162	2.39%
Hysol 9361	Elastic Modulus (psi)	1132056± 13051	1.19%
	Poisson's Ratio	0.353 ± 0.016	4.55%
	Maximum Stress (psi)	4225± 201	4.76%

Figure 34: Young modulus and Poisson ratio of epoxies at room temperature and at 100 K [66]

and back to room temperature for five minutes. In some cases the samples underwent two weeks at 1.8 K, three days at 4.2 K, one week at room temperature, sometimes under a stress of 15 MPa. The effect of temperature on shear strength is reported in Fig. 35.

Temperature effect on the shear strength (MPa)

	M 722 XD 4447	M 723 AZ 15	M 724 AW 106	M 725 2850 FT
Initial value at 293 K	25.8	26.4	21.1	16.9
Initial value at 77 K	40.3	17.6	18.3	23.0
After *n* cycles	*n* = 40	*n* = 10	*n* = 10	
at 293 K	22.2	23.1	20.4	n.m.
at 77 K	39.6	19.5	21.3	n.m.

Figure 35: Shear strength at room temperature and at 77 K for three Araldites and Stycast 2850 FT [68]

The performances of some adhesives for bonding composites and aluminum has been investigated by [69] at room temperature and at -150^0 C using double lap joints. The adhesives were Bondex606, Loctite EA9696, Cyanamid FM 73. The joint strength was larger at lower temperature (Fig. 36, left) for all adhesives, with the largest increase for the sample with lower strength at room temperature. Performances at room temperature are not necessarily predictive of the performances at lower temperatures. The strength and the stiffness of the adhesive generally show an increase at lower temperature (Fig. 36, right).

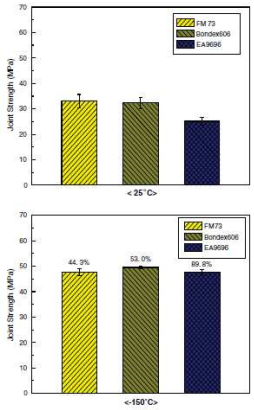

	RT	−50 °C	−100 °C	−150 °C
(a) Stiffness				
Bondex606	2.8	3.6	5.0	6.3
EA9696	1.9	2.4	3.9	5.5
FM73	2.5	3.2	4.5	5.5
Aluminum	68.5	70.6	72.0	74.1
(b) Strength				
Bondex606	39.4	47.8	43.1	49.3
EA9696	33.9	50.0	53.8	46.4
FM73	45.7	73.3	54.0	57.4
Aluminum	294.6	313.5	321.3	350.5

Figure 36: Joint strength at room temperature and at -150^0 C (left) and strength and stiffness (right) for three adhesives [69]

As discussed above, adhesives can be cured at room temperature or higher. The work by [63] has shown that the temperature and the duration of curing is crucial for the bonding strength. The work by [70] has investigated the strength and the thermal residual stress of epoxy XB 5032A/B at cryogenic temperatures versus the cure cycle.

The adhesive peel strength at room temperature and at -150^0 C increased with increasing curing temperature. On the other hand, when the adhesive was cured at room temperature, the strength at cryogenic temperature halved, suggesting that high temperature curing is recommended. A special cure cycle was devised, made of quick cooling and reheating steps, producing an increase of the adhesive strength and a decrease of the cure time.

5.2.2 Thermal expansion coefficient

There are some experimental data available.

The thermal expansion coefficient has been measured for Hysol 9361, Tra-Con F113, Epotek 301-2 by [66]. The experimental apparatus was a liquid nitrogen cryostat equipped with a LVDT to measure the variation in sample length. The integral fractional change in length of the samples versus the temperature is shown in Fig. 37.

Ambient Temperature		
Tra-Con F113 dL/L ($\times 10^{-3}$)	–	–
Epotek 301-2 dL/L ($\times 10^{-3}$)	–	–
Hysol 9361 dL/L ($\times 10^{-3}$)	–	–
250 K		
Tra-Con F113 dL/L ($\times 10^{-3}$)	-3.27 ± 0.13	3.94%
Epotek 301-2 dL/L ($\times 10^{-3}$)	-2.83 ± 0.04	1.52%
Hysol 9361 dL/L ($\times 10^{-3}$)	-4.69 ± 0.04	0.8%
200 K		
Tra-Con F113 dL/L ($\times 10^{-3}$)	-6.20 ± 0.11	1.73%
Epotek 301-2 dL/L ($\times 10^{-3}$)	-5.45 ± 0.03	0.59%
Hysol 9361 dL/L ($\times 10^{-3}$)	-8.69 ± 0.02	0.3%
150 K		
Tra-Con F113 dL/L ($\times 10^{-3}$)	-8.71 ± 0.06	0.76%
Epotek 301-2 dL/L ($\times 10^{-3}$)	-7.70 ± 0.11	1.37%
Hysol 9361 dL/L ($\times 10^{-3}$)	-11.3 ± 0.003	0.2%
100 K		
Tra-Con F113 dL/L ($\times 10^{-3}$)	-10.7 ± 0.08	0.72%
Epotek 301-2 dL/L ($\times 10^{-3}$)	-9.66 ± 0.18	1.88%
Hysol 9361 dL/L ($\times 10^{-3}$)	-13.3 ± 0.03	0.2%

Figure 37: Integral fractional change in length for Hysol 9361, Tra-Con F113, Epotek 301-2 [66]

The thermal expansion coefficient of Bondex606, Loctite EA9696, Cyanamid FM 73 has been investigated by [69] down to -150 ^{0}C. The coefficient is shown in Fig. 38.

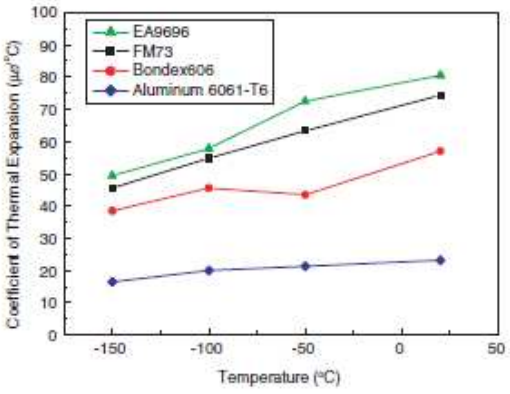

Figure 38: Thermal expansion coefficient of Bondex606, Loctite EA9696, Cyanamid FM 73 [69]

5.2.3 Thermal conductivity

There are a few experimental measurements of thermal conductivity of epoxy systems at cryogenic temperatures, see [71] for Stycast 2850FT. The authors of [72] have tested four epoxies: Stycast 2850 FT, Poxycomet F, DP190, Eccobond 285 in the range 4.2–10 K. The samples were in vacuum and were mounted between a cold heat sink to a cryogenic liquid bath and a heat source. The temperature was measured with a germanium resistance thermometer. The thermal conductivity is in the range 0.02÷0.1 W/m K in the interval 4–10 K (Fig. 39).

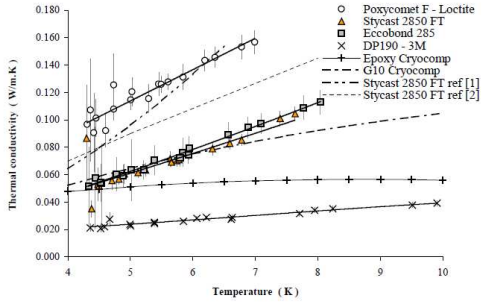

Figure 39: Thermal conductivity of Stycast 2850 FT, Poxycomet F, DP190, Eccobond 285 [72]

5.2.4 Open problems

The two aspects where literature is scarce are the aging and the contamination of adhesives. Both items involve dedicated long duration testing. The work by [63] suggested that aged epoxies have poorer performances compared to freshly prepared ones. In addition, we must consider the aging of successful bonding during the long foreseen operation of cryogenic operation of Einstein Telescope.

The issue of contamination has been addressed, for some adhesives, by the NASA outgassing database [73]. The NASA outgassing program follows the ASTM E-595 screening method to determine the volatile content of materials in vacuum at 125 ^{0}C. The allowed level of contamination is a total mass loss (TML) of 1% and a total collected volatile condensable material (CVCM) of 0.1%. The results available for some adhesives mentioned in the present reportare listed in Tab. 2 [73]. The spread of performances is caused by the test of samples with different curing temperature and/or curing time: the preparation has an impact on the final outgassing.

Table 2: TML and CVCM of some adhesives of potential interest for cryogenic operation of Einstein Telescope [73]

Material	%TML	%CVCM
Stycast 1266	1.41	0.12
Stycast 2850FT	0.19–1.14	0.00–0.34
Eccobond 285	0.28–2.46	0.00–1.00
Armstrong A–12	0.53–4.22	0.00–0.65
Armstrong A–31	0.44–1.51	0.01–0.22
3M Scotchweld 2216 B/A	0.10–2.85	0.00–0.54
Epibond 1210A/9615A	0.77	0.02
Tra–Con F113	1.82	0.11
Aremco 517	0.91	0.04

5.3 Conclusions

The use of adhesives in cryogenic operation of Einstein Telescope requires some dedicated investigations. Assuming that the required bond strength is defined for the various applications, it could be necessary to optimize the combination of adhesive and materials to be bonded. The critical application of magnet mounting on mirror will require an investigation on a possible impact on the quality factor of the mirror. The foreseen long operation of cryogenic operation of Einstein Telescope will involve the aging of adhesives and their ability to tolerate thermal cycling. An issue to be defined is the maximum tolerated contamination. The literature about cryogenic properties and performances of adhesives is growing. Some trends are however clear: the properties of adhesives depend on the specific production batch and on the recipe (time and temperature) for curing. Since the performances measured at room temperature are not necessarily predictive of the performances at lower temperatures, it is suggested that the tests are performed at the temperature of operation.

6 Magnets

Cryogenic operation of Einstein Telescope will require the use of permanent magnets in different parts. The properties of permanent magnet materials are strongly dependent on temperature [74]. The purpose of this note is to review the properties of some candidate magnetic materials below room temperature. The properties of some materials have been summarized by [74]. The basic quantities defining the magnet characteristics are [75]:

- B_r: residual magnetization
- H_{ci}: intrinsic coercive field
- $(BH)_{max}$: energy product

For most materials, the residual magnetization, the intrinsic coercive field and the energy product increase with decreasing temperature [74]. The traditional magnetic materials are: ferrite, Alnico, Neodymium–Iron–Boron (NdFeb), Samarium–Cobalt (SmCo). The characteristics of main magnetic families [76] are shown in Fig. 40.

	Ferrite	Alnico	SmCo			NdFeB	
Property	Ceramic 8	Alnico 5	1-5	1-5 TC	2-17	Bonded	Sintered
B_r (kG)	4.0	12.5	9.0	6.1	10.4	6.9	13.4
α (%/°C)	-0.18	-0.02	-0.045	-0.001	-0.035	-0.105	-0.12
$(BH)_{max}$ MGOe	3.8	5.5	20	9	26	10	43
H_{ci} (kOe)	3.3	0.64	30	30	25	9	15
β (%/°C)	+0.4	-0.015	-0.3	-0.02	-0.3	-0.4	-0.6
H_s (kOe)	10	3	20	40	30	35	35
T_c (°C)	460	890	727	729	825	360	310

Notes:
The quantity α is the reversible temperature coefficient of B_r. (20 °C to 100 °C minimum)
The quantity β is the reversible temperature coefficient of H_{ci}. (20 °C to 100 °C minimum)
The field required to saturate the magnet is H_s.
TC means temperature compensated. [References 1, 2]

Figure 40: Main characteristics of magnets for possible cryogenic use [76]

We will include in our discussion also some new generation magnetic materials: Mn–Al–C, Praseodymium–Iron–Boron (PrFeB).

6.1 Ferrite

Ferrites are an exception in the scenario of magnets, since the intrinsic coercivity decreases with decreasing temperature, with irreversible losses after operation at -60 ^{0}C [74], [77]. Thus ferrites are not recommended below this temperature. The demagnetization curves of ferrite ceramics at different temperatures are shown in Fig. 41.

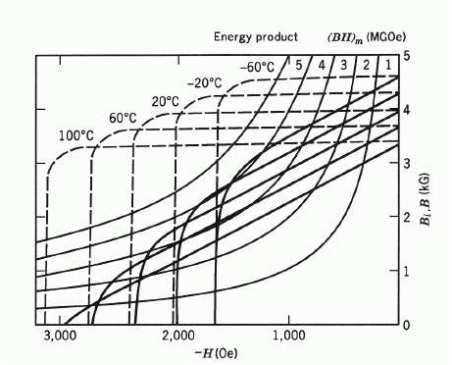

Figure 41: Demagnetization curves of Ceramic 5 at different temperatures [74]

6.2 Alnico and Mn–Al–C

Alnico has a low temperature coefficient for the quantity B_r. An irreversible loss of magnetization of about 10% has been observed after operation at -190 ^{0}C [74], [77]. The lowest suggested operation temperature for Alnico is -75 ^{0}C. The demagnetization curves of Alnico at different temperatures are shown in Fig. 42.

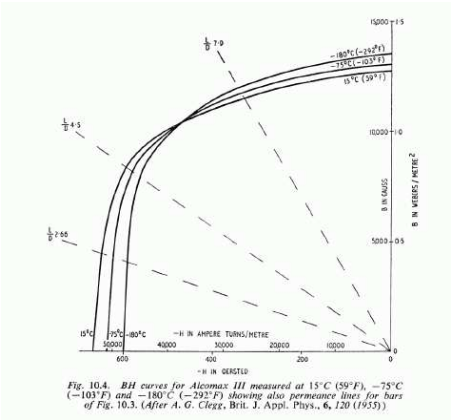

Figure 42: Demagnetization curves of Alnico 5 at different temperatures [74]

A possible replacement for Alnico is Mn–Al–C, a material less brittle than ferrite or Alnico. The residual magnetization is similar to Alnico one, while the coercive field is similar to the one of ferrites. The properties of Mn–Al–C between -50 and 150 ^{0}C haves been investigated by [78]. The remanent field and coercivity increase with decreasing temperature (Fig. 43).

6.3 Neodymium–Iron–Boron and Praseodymium–Iron–Boron

Neodymium–Iron–Boron (NdFeB) shows an initial increase of residual field with decreasing temperature, but a decrease below about 140 K because of spin reorientation [74], [79]. A variant is Praseodymium–Iron–Boron (PrFeB) where Pr replaces Nd. Several investigation of NdFeB and PrFeB magnets have been performed in the context of undulators for synchrotron facilities. NdFeB and PrFeB magnets have been tested down to liquid nitrogen temperature by [80]. The authors tested Neodymium–Iron–Boron (NdFeB) magnets (types NEOMAX 35EH and 50 BH) and a Praseodymium–Iron–Boron (PrFeB) magnet (type 53CR). The two types of NdFeB magnets achieved the maximum of remanent field at different temperatures, undergoing a sharp decrease below

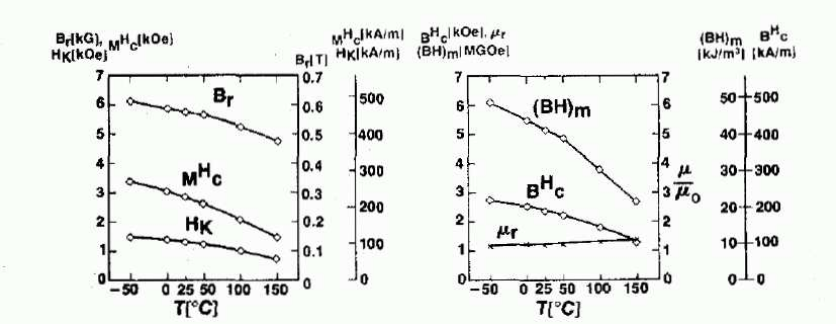

Figure 43: Magnetic properties of Mn–Al–C at different temperatures [78]

the maximum. The remanent field of PrFeB increased with decreasing temperature (Fig. 44, left). On the other hand, the coercivity of all magnets increased with decreasing temperatures (Fig. 44, right).

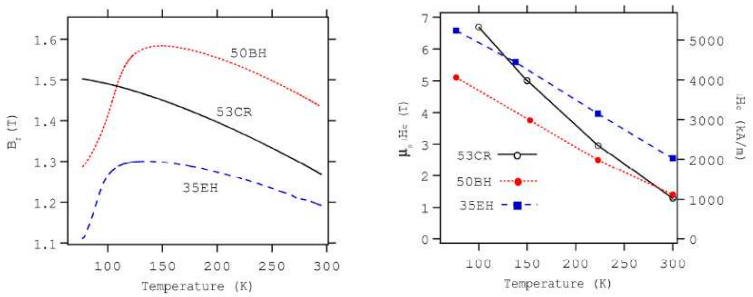

Figure 44: NdFeB (35EH and 50 BH) and PrFeB magnets (53CR) [80]: temperature behavior of the remanent field (left); temperature behavior of the coercivity (right)

A further comparison of NdFeB and PrFeB magnets has been performed by [81], who tested NdFeB (NEOMAX 50BH, 48H, 35EH, 27VH) and PrFeB (NEOMAX 35CR). The measurements of NdFeB magnets showed close values of peak remanent field and a sharp decrease below. The remanent field of PrFeB steadily increased with decreasing temperature (Fig. 45, left). On the other hand, the coercivity of all magnets increased with decreasing temperatures (Fig. 45, right). The NEOMAX 35EH variety has been extensively tested by [82].

A similar investigation has been performed by [83] with NdFeB samples of type NEOREM 595t (Fig. 46). The maximum remanent field occurred close to 110 K, lower than the values reported in previous investigations. The suggested cause was the presence of dysprosium in the NdFeB material.

A study by [84] compared the properties of NdFeB samples of type NEOREM 495T with the types BH50, VAC764, N50. The maximum remanent field occurred in the region between 100 and 110 K, while coercivity was improving with decreasing temperature (Fig. 47).

More recently, different varieties of magnets based on neodymium, Iron and Boron, but including other elements, have been developed. The materials based on $(Nd_xPr_{1-x})_{12.9}Dy_{0.4}Fe_{74.3}Co_{6.7}B_{5.7}$ with x=0.5 have shown better magnetic properties at 78 K compared to $Pr_2Fe_{14}B$ [85]. The maximum energy product behavior versus temperature of different samples is shown in Fig. 48.

6.4 Samarium–Cobalt

Samarium–Cobalt magnets have a magnetic strength almost three times larger than the one of ferrites at room temperature. Samarium–Cobalt magnets have been tested by Virgo for outgassing; the outgassing properties

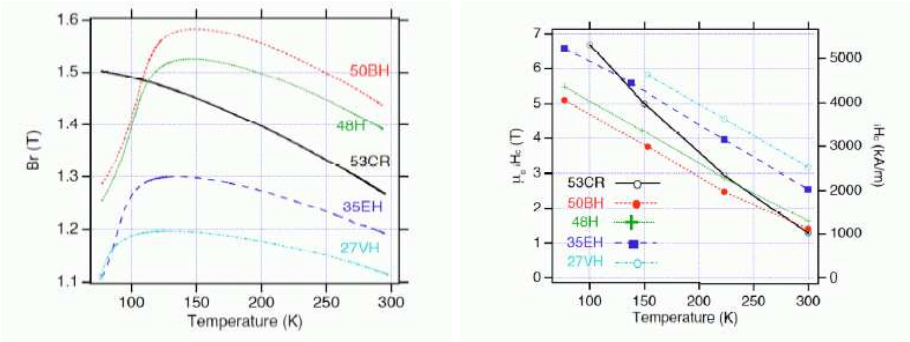

Figure 45: NdFeB (NEOMAX 50BH, 48H, 35EH, 27VH) and PrFeB (NEOMAX 35CR) magnets [81]: temperature behavior of the remanent field (left); temperature behavior of the coercivity (right)

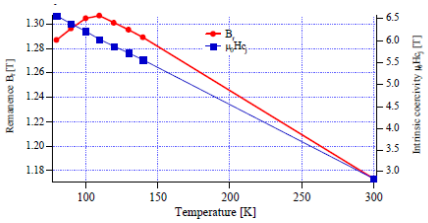

Figure 46: Remanent field and intrinsic coercivity for NEOREM 595t against temperature [83]

are better by two orders of magnitude compared to ferrite [86], [87], [88], [89], [90]. Samarium–Cobalt (varieties $SmCo_5$ and Sm_2Co_{17}) shows very small losses with decreasing temperature down to 4 K and has been successfully used down to 2 K [74]. The intrinsic coercive force of some SmCo samples shown in Fig. 49 exhibits an increase with decreasing temperatures [91].

A comparison of the magnetization properties of Samarium–Cobalt and neodymium–Iron–Boron at cryogenic temperatures has been performed by [92], in the context of the operation of a gallium doped p-Ge laser in the environment of cryogenic permanent magnets. The temperature dependence of the magnetic field of NdFeB and SmCo magnets is shown in Fig. 50. While the magnetic field of SmCo decreases only by a few percent, the field of NdFeB, after an initial fast increase, shows a strong decrease below 100 K.

Another comparison of NdFeB and SmCo magnets has been performed by [93]. The samples were NdFeB type NEOMAX 35EH, 48H, 50BH, PrFeB type NEOMAX 53CR, Sm_2Co_{17} type VACOMAX 240 HR. The NdFeB magnets showed a peak of remanent field between 110 and 140 K and a sharp decrease below the maximum. The remanent field of PrFeB and Sm_2Co_{17} steadily increased with decreasing temperature (Fig. 51, left). On

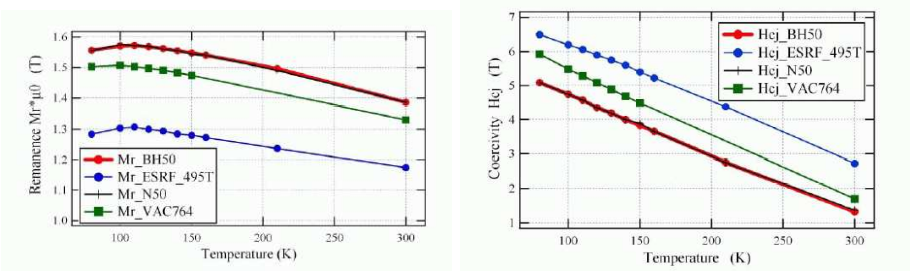

Figure 47: Remanent field (left) and intrinsic coercivity (right) versus temperature for NEOREM 495T, BH50, VAC764, N50 [84]

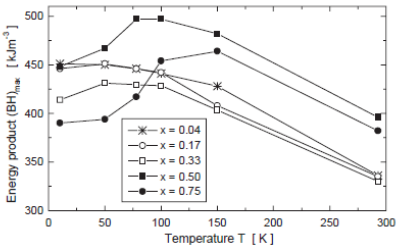

Figure 48: Maximum energy product versus temperature of (Nd,Pr)(Fe,Co)B magnets versus the Nd-content [85]

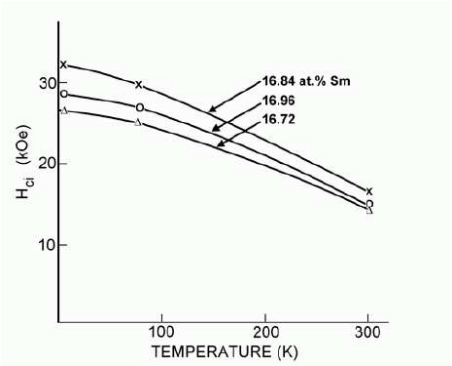

Figure 49: Coercive field of Samarium–Cobalt magnets [91]

the other hand, the coercivity of all magnets increased with decreasing temperatures (Fig. 51, right).

Some varieties of Samarium–Cobalt magnets ($SmCo_5$, $(Sm,Pr)Co_5$, Sm_2Co_{17}) have been test between -60 ^{0} and 200 ^{0}C by [94]. The various labels in the caption identify different ways of preparing magnets. The properties of different materials at room temperature are summarized in the left part of Fig. 52. The temperature dependence of the magnetic properties is shown in the right part of Fig. 52. The residual induction B_r decreases more quickly on heating for the isostatically pressed $SmCo_5$, than for the same compound pressed in transverse field. The same behavior is observed for the quantity $(BH)_{max}$. The Sm_2Co_{17} material shows similar temperature coefficients for varieties pressed orthogonally and parallel to the aligning field.

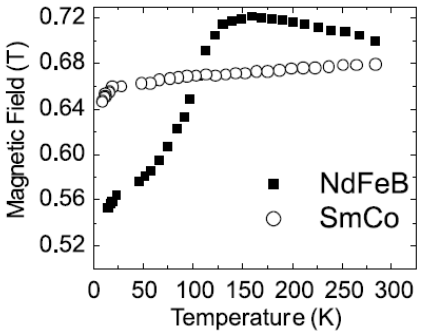

Figure 50: Temperature dependence of the magnetic field of NdFeB and SmCo [92]

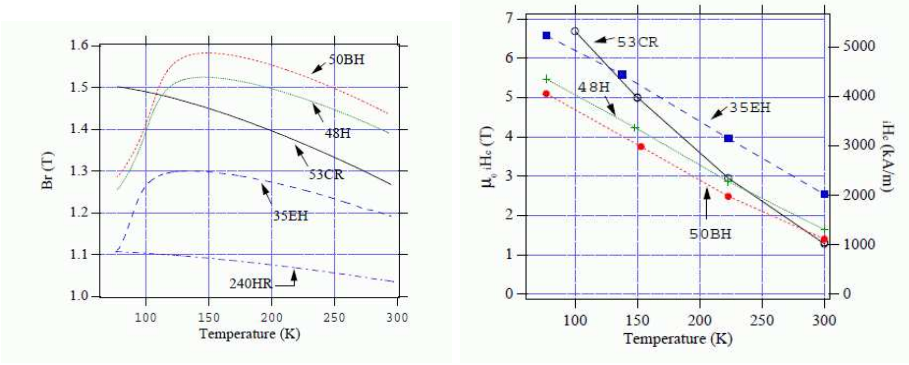

Figure 51: NdFeB magnets (NEOMAX 35EH, 48H, 50BH), PrFeB magnet(NEOMAX 53CR), Sm_2Co_{17} (VACOMAX 240HR) [93]: temperature behavior of the remanent field (left); temperature behavior of the coercivity

TABLE I - PERTINENT ROOM-TEMPERATURE PROPERTIES OF TEST SAMPLE GROUPS

AVERAGE PROPERTIES AT 25° C

	$Sm Co_5$ P⊥M	$Sm Co_5$ I	$(Sm, Pr)Co_5$ P⊥M	$Sm_2(Co, TM)_{17}$ P // M	$Sm_2(Co, TM)_{17}$ P⊥M	$Sm(Co, Fe, Cu)_7$ P⊥M
B_r [kG]	8.90	10.02	9.67	9.99	10.82	9.45
$_BH_c$ [kOe]	8.69	9.22	8.82	6.05	6.04	7.44
$_MH_c$ [kOe]	23.84	16.80	11.55	7.12	6.55	8.13
$(BH)_{max}$ [MGOe]	19.7	23.5	21.8	22.0	27.2	21.9
H_K [kOe]	13.20	10.68	9.48	4.71	5.20	6.73

FABRICATION METHODS: [P⊥M] DIE PRESSED WITH FORCE PERPENDICULAR TO MAGNETIC ALIGNING FIELD. [I] ISOSTATICALLY PRESSED. [P//M] DIE PRESSED WITH FORCE AND FIELD PARALLEL. (*) TM IS ONE OR SEVERAL TRANSITION METALS (Fe, Cu, Zr, Hf).

TABLE II. TEMPERATURE DEPENDENCE OF MAGNETIC PROPERTIES
(Percent change from values at 25°C)

Permanent Magnet Property	Temp. of Measmt. [°C]	COMPOSITION TYPE OF SINTERED MAGNET MATERIAL* $SmCo_5$ P⊥M	$SmCo_5$ I	$(Sm, Pr)Co_5$ P⊥M	$Sm_2(Co, TM)_{17}$ P⊥M	$Sm_2(Co, TM)_{17}$ P//M	$Sm(Co, Cu, Fe)_7$ P⊥M
Change from 25°C →		Δ [%]	Δ [%]	Δ [%]	Δ [%]	Δ [%]	Δ [%]
B_r	- 60	+ 5.6	+ 4.1	+ 5.0	+ 2.4	+ 2.6	+ 2.3
	+ 100	- 2.5	- 3.6	- 3.4	- 1.0	- 0.8	- 2.0
	+ 200	- 6.3	- 9.1	- 8.8	- 4.7	- 5.0	- 6.5
$_BH_c$	- 60	+ 6.6	+ 7.3	+ 7.8	+13.0	+10.9	+ 11.5
	+ 100	- 4.2	- 8.9	- 11.1	- 16.2	- 15.7	- 11.6
	+ 200	- 14.3	- 27.6	- 43.1	- 32.7	- 32.9	- 27.0
$(BH)_{max.}$	- 60	+ 12.1	+ 12.2	+ 11.8	+ 8.1	+ 9.8	+ 6.1
	+ 100	- 5.1	- 8.7	- 7.3	- 5.9	- 10.6	- 5.8
	+ 200	- 14.8	- 27.9	- 22.8	- 27.9	- 29.5	- 19.3
H_K	- 60	+20.9	+26.8	+25.2	+15.7	+16.0	+19.1
	+ 100	-20.7	-27.5	-22.2	- 19.6	- 22.7	- 14.9
	+200	-45.2	- 65.6	- 54.0	- 39.6	- 45.5	- 32.8
$_MH_c$	- 60	+11.5	-17.0	+23.9	+ 14.4	+ 13.6	+ 15.0
	+ 100	- 20.2	-20.6	- 23.2	- 15.3	- 16.1	- 12.4
	+ 200	- 45.9	-49.8	- 54.1	- 32.5	- 34.4	- 29.4

Fabrication Methods: [P⊥M] Die pressed with force perpendicular to magnetic aligning field. [I] Isostatically pressed. [P//M] Die pressed with force and field parallel. (*) TM is one or several transition metals (Fe, Cu, Zr, Hf)

Figure 52: Room temperature properties (left) and temperature dependence of magnetic properties (right) of samples measured by [94]

6.5 Conclusions

We have shown that there are some candidates for possible operation at cryogenic temperatures. Further investigations are required before selecting the magnets, defining the operation temperature, possible necessity of high temperature baking, maximum allowed contamination. NdFeB and SmCo are the suggested choices below room temperature. The latter shows the best properties at low temperatures. In addition, it is able to undergo baking at higher temperatures. We have also shown that inside the same class of material, there is a spread of magnetic properties of specific trademarks.

7 Conclusions

We have seen that several components and materials are potentially suitable for use in Einstein Telescope. Careful testing is needed. Generally room temperature performances cannot be scaled at cryogenic temperatures. Even for materials and components described in literature, there is a spread of properties depending on sample fine characteristics, processing history etc.

References

[1] G. K. White, "Experimental Techniques in Low–temperature Physics", Clarendon Press, 1968 1, 5

[2] F. Pobell, "Matter and Methods at Low Temperatures", Springer–Verlag, 1992 1, 2, 5, 21

[3] Reed, Clarke, "Materials at low temperature" 1, 3, 5, 6

[4] K. Kasahara et al., 28th International Cosmic Ray Conference, pg. 3115 3

[5] T. Tomaru et al., *Phys. Lett. A* **301** (2002) 215 6

[6] S. Kanagaraj and S. Pattanayak, *Cryogenics* **43** (2003) 399 7

[7] R. Grossinger and H. Muller, *Rev. Sci. Instr.* **52** (1981) 1528 7, 8

[8] F. R. Kroegner and C. A. Swenson, *J. Appl. Phys.* **48** (1977) 853 7, 8

[9] R. H. Carr and C. A. Swenson, *Cryogenics* **4** (1964) 76 7, 8

[10] D. N. Batchelder and R. O. Simmons, *J. Chem. Phys.* **41** (1964) 2324 7, 8

[11] J. K. Tien and C.–T. Yen 7, 9

[12] M. Beccaria et al., *Nucl. Instrum. Meth. A* **404** (1998) 455 9

[13] T. Uchiyama et al., *Phys. Lett. A* **273** (2000) 310 10

[14] T. Uchiyama et al., *Phys. Lett. A* **261** (1999) 5 10

[15] C. J. Yeager and S. S. Courts, *IEEE Sensors J.* **4** (2001) 352 11

[16] V. Datksov et al., 16th IEEE Particle Accelerators Conference (PAC 95) and International Conference on High Frequency Accelerators (IUPAP), Dallas, 1–5 May 1995, Vol. 3, pg. 20304 12

[17] J. Casas et al., LHC Project Report 333, presented at the 1999 Cryogenic Engineering and International Cryogenic Materials Conference (CEC–ICMC'99), 12–16 July 1999, Montreal, Canada 12

[18] J. Ylöstalo et al., *Cryogenics* **36** (1996) 1033 12, 13

[19] S. Miyoki et al., *Cryogenics* **40** (2000) 61 13

[20] S. Miyoki et al., *Cryogenics* **41** (2001) 415 13

[21] T. Tomaru et al., *Cryogenics* **44** (2004) 309 13, 14

[22] E. T. Swartz, *Rev. Sci. Instrum.* **57** (1986) 2848 14, 15

[23] Phytron 15, 16

[24] Mission Research Corporation 15, 16

[25] Empire Magnetics Inc. 15, 16

[26] Maxon Motor 16, 17

[27] Donovan Micro–Tek 16, 17

[28] New Scale Technology 16, 17

[29] N. Sato et al., *Cryogenics* **43** (2003) 425 17, 18

[30] Arun Microelectronics 17

[31] Dicronite 18

[32] RBC Specialty Bearings 18

[33] RMB Bearings 18

[34] AEA Technology – ESTL 18

[35] Cryogenic Data Handbook 21, 22

[36] M. Bernardini and R. Poggiani, VIR-TRE-PIS-3400-115, Outgassing test of cabling with Pyre-ML insulation, 21/4/1997 21

[37] M. Bernardini and R. Poggiani, VIR-TRE-PIS-3400-116, Outgassing test of a Gore-Tex ribbon, 21/4/1997 21

[38] M. Bernardini et al., VIR-TRE-PIS-3400-51 (VACPISA 037), Outgassing measurements of alumina insulated cables, 15/2/1996 21

[39] M. Bernardini et al., VIR-TRE-PIS-3400-52 (VACPISA 036), Outgassing measurements of Kapton insulated cables, 15/2/1996 21

[40] M. Bernardini and R. Poggiani, VIR-TRE-PIS-3400-112, Installation of a second vacuum chamber for small samples and test of a Kapton ribbon cable, 21/4/1997 22

[41] M. Bernardini et al., VIR-TRE-PIS-3400-137, Outgassing test of an Axon Kapton ribbon 22

[42] D. J. Benford et al., *Cryogenics* **39** (1999) 93 22

[43] A. Kushino et al., *Cryogenics* **45** (2005) 637 22

[44] D. E. Glass et al., *Cryogenics* **38** (1998) 983 23

[45] R. S. Bathia et al., *Cryogenics* **41** (2002) 851 23

[46] R. C. Richardson and E. N. Smith, *Experimental Techniques in Condensed Matter Physics at Low Temperatures*, Addison-Wesley (1988) 25

[47] Emerson & Cumming Inc. 25

[48] N. Saito et al., *Cryogenics* **43** (2003) 425 25

[49] Loctite 25, 26

[50] Composite Technology Inc. 26, 29

[51] Master Bond Inc. 26

[52] Armstrong Epoxy Adhesives, Resin Technology Group INC. 26

[53] PRC De Soto International 26

[54] 3M 26

[55] O. P. Anashkin et al., *Cryogenics* **39** (1999) 795 26

[56] Cotronics Corp. 26

[57] S. Bhawnik et al., *Int. J. Adh. Adhes.* **26** (2006) 400 26

[58] Aremco 26

[59] M. Bernardini and R. Poggiani, VIR-TRE-PIS-3400-120, 21/4/1997 26

[60] M. Bernardini, H. B. Pan and R. Poggiani, VIR-TRE-PIS-3400-140, 16/1/1999 26

[61] S. Lee et al., *Surf. Sci.* **578** (2005) 5 26

[62] Sauereisen 26

[63] I. F. Silvera et al., *Rev. Sci. Instr.* **73** (2002) 2108 27, 28, 29, 31

[64] C. Echols and K. Bui, KIRMOS note KTP0300 27

[65] C. Echols, KIRMOS note KTP0600 27, 28

[66] H. Cease et al., Fermilab-TM-2366-A 28, 29, 30

[67] N. Albritton and W. Young, *Cryogenics* **36** (1996) 713 29

[68] M. Tavlet and L. Hominal, *Cryogenics* **38** (1998) 47 29

[69] S.–G. Kang et al., *Comp. Struct.* **78** (2007) 440 (2007) 440 29, 30, 31

[70] K. H. Lee and D. G. Lee, *Comp. Struct.* **86** (2008) 37 29

[71] C. L. Tsai et al., *Cryogenics* **18** (1978) 562 30

[72] F. Rondeaux et al., I–01C–02, Cryogenic Engineering Conference, July 16–20, 2001, Madison, USA 30, 31

[73] NASA outgassing data for selecting spacecraft materials 31, 32

[74] Arnold technote 32, 33, 34, 35

[75] S. R. Trout, Proc. Electric Manufacturing and Coil Winding Conference 2000 (2000) 32

[76] S. R. Trout, Proc. Electric Manufacturing and Coil Winding Conference 2001 (2001) 32, 33

[77] R. J. Parker and R. J. Studders, Permanent Magnets and Their Application, John Wiley and Sons (1962) 32, 33

[78] Z. A. Abdelnour et al., *IEEE Trans. Magn. MAG-17* (1981) 2651 33, 34

[79] L. Garcia et al., *Phys. Rev. Lett.* **85** (2000) 429 33

[80] T. Hara et al., *PhysRevSTAB* **7** (2004) 050702 33, 35

[81] H. Kitamura et al., Proceedings of EPAC 2004, Lucerne, Switzerland, 59 (TUYBCH01) 33, 35

[82] T. Tanaka et al., *New J. Phys.* **8** (2006) 287 34

[83] C. Kitegi et al., Proceedings of EPAC 2006, Edinburgh, Scotland, 3559 (THPLS119) 34, 35

[84] C. Benabderrahmane et al., Proceedings of EPAC08, Genoa, Italy, 2225 (WEPC098) 34, 36

[85] D. Hinz et al., *J Magn. Magn. Mat. 272-276* (2004) e321 34, 36

[86] M. Bernardini et al., VIR-TRE-PIS-3400-58 (VACPISA 047), 15/6/1996 34

[87] M. Bernardini et al., VIR-TRE-PIS-3400-57 (VACPISA 046), 15/4/1996 34

[88] M. Bernardini et al., VIR-TRE-PIS-3400-61 (VACPISA 050), 15/7/1996 34

[89] M. Bernadini and R. Poggiani, VIR-TRE-PIS-3400-118, 21/4/1997 34

[90] M. Bernardini, H. B. Pan and R. Poggiani, VIR-TRE-PIS-3400-139, 16/1/1999 34

[91] S.R. Trout and C.D. Graham, Jr., AIP Conference Proceedings, vol. 29 (1975) 608 35, 36

[92] C. J. Fredricksen et al., *Infr. Phys. Tech.* **44** (2003) 79 35, 37

[93] T. Hara et al., Proceedings of APAC 2004, Gyeongju, Korea, 216 (TUM102) 35, 37

[94] Z. A. Abdelnour et al., *IEEE Trans. Magn. MAG-16* (1980) 994 36, 38